Master's thesis

Master's Programme in Data Science

Learning the road conditions

Jussi-Pekka Martikainen

June 1, 2019

Supervisor(s): Associate Professor Laura M. Ruotsalainen

Examiner(s): Associate Professor Petteri Nurmi
Associate Professor Laura M. Ruotsalainen

University of Helsinki
Faculty of Science

P. O. Box 68 (Pietari Kalmin katu 5)
00014 University of Helsinki

HELSINGIN YLIOPISTO — HELSINGFORS UNIVERSITET — UNIVERSITY OF HELSINKI

Tiedekunta — Fakultet — Faculty	Koulutusohjelma — Utbildningsprogram — Degree programme
Faculty of Science	Master's Programme in Data Science

Tekijä — Författare — Author

Jussi-Pekka Martikainen

Työn nimi — Arbetets titel — Title

Learning the road conditions

Työn laji — Arbetets art — Level	Aika — Datum — Month and year	Sivumäärä — Sidantal — Number of pages
Master's thesis	June 1, 2019	88

Tiivistelmä — Referat — Abstract

Wood is the fuel for the forest industry. Fellable wood is collected from the forests and requires transportation to the mills. The distance to the mills is quite often very long. The most used long-distance transportation means of wood in Finland is by road transportation with wood-trucks. The poor condition of the lower road network increases the transportation costs not only for the forest industry but for the whole natural resources industry. Timely information about the conditions of the lower road network is considered beneficial for the wood transportation and for the road maintenance planning to reduce the transportation related costs. Acquisition of timely information about the conditions of the lower road network is a laborious challenge to the industry specialists due to the vast size of the road network in Finland. Until the recent development in ubiquitous mobile computing collecting the road measurement data and the detection of certain road anomalies from the measurements has traditionally required expensive and specialized equipment. Crowdsensing with the capabilities of a modern smartphone is seen as inexpensive means with high potential to acquire timely information about the conditions of the lower road network. In this thesis a literature review is conducted to find out the deteriorative factors behind the conditions of the lower road network in Finland. Initial assumptions are drawn about the detectability of such factors from the inertial sensor data of a smartphone. The literature on different computational methods for detecting the road anomalies based on the obtained accelerometer and gyroscope measurement data is reviewed. As a result a summary about the usability of the reviewed computational methods for detecting the reviewed deteriorative factors is presented. And finally suggestions for further analysis for obtaining more training data for machine learning methods and for predicting the road conditions are presented.

ACM Computing Classification System (CCS):
Computing methodologies → Machine learning → Machine learning approaches
Human-centered computing → Ubiquitous and mobile computing → Ubiquitous and mobile computing systems and tools
Applied computing → Operations research → Transportation

Avainsanat — Nyckelord — Keywords

accelerometer, gyroscope, machine learning, road conditions

Säilytyspaikka — Förvaringsställe — Where deposited

Muita tietoja — Övriga uppgifter — Additional information

Contents

1. Introduction

Roundwood is the basic raw material utilized by the forest industry. Roundwood is harvested from the forests and then transported to the mills. The transportation of domestic roundwood is done either by floating, railways or roads as the distance between the fellable forests and the mills can be long. The long-distance transportation of industrial roundwood is important part of the raw material supply chain for the forest industry. Out of the different long-distance transportation means of industrial roundwood the road transportation has historically been in a major role in Finland since the 1960's according to Strandström [28].

In 2017 the total long-distance transportation volume of domestic wood to mill was 48 627 k-m^3 (thousand solid cubic metres) with the mean distance of 159 km as shown in Table 1.1 [28]. From the total long-distance transportation volume 75,2 % was transported by road with the mean distance of 105 km, 22,6 % by railway with the mean distance of 323 km and 2,2 % by water transportation with the mean distance of 287 km. From the volume delivered by railway 21,4 units of percentage was delivered by road-to-railway with the mean distance of 49 km and from the volume delivered by water 1,8 units of percentage was delivered by road-to-floating with the mean distance of 43 km. This equals in 98,5 % of the total volume of industrial wood with the mean distance of 92 km was delivered by road either partly or as a whole.

The total cost of long-distance transportation of industrial roundwood in 2017 was 395,9 MEUR (million euros) in Finland as is shown in the Table 1.2 [28]. The 326,4 MEUR total cost of road transportation is clearly the biggest cost factor with 82 % of the total long-distance transportation costs. From the Table 1.1 it can be seen that the average unit costs of the total long-distance transportation volume of industrial roundwood was 5,1 c/m^3-km or 8,14 EUR/m^3. The unit costs of long-distance transportation by road-to-mill was 7,1 c/m^3-km or 7,4 EUR/m^3. The unit costs of railway and water transportation are elevated by the unit costs of road-to-railway and road-to-floating respectively. With this the total unit costs of road transportation was 7,4 c/m^3-km or 6,81 EUR/m^3.

Road network, infrastructure and loading terminals were found as one of the most significant problem areas for the cost-efficient long-distance road transportation

Table 1.1: Long-distance Transportation of Roundwood, 2017 [28].

	Domestic roundwood				
	1 000 m^3	%	km	cent/m^3km	€/m^3
Total long-distance transportation	48 627		159	5,1	8,14
Total by road	47 897	98,5	92	7,4	6,81
By road-to-mill	36 549	75,2	105	7,1	7,45
Rail transportation sequence	10 989	22,6	323	3,2	10,16
By road-to-railway	10 430	21,4	49	9,9	4,80
Rail transportation	10 989	22,6	274	2,1	5,68
Water transportation sequence	1 089	2,2	287	3,6	10,26
By road-to-floating/barge	918		43	10,1	4,42
Water transportation	1 089		243	2,7	6,53

Table 1.2: Cost and timber volume, 2017 [28].

	Mill. €	%	Mill. m^3	Mill. m^3km	%
Harvesting	424.8		40.1		
Long-distance transportation	395,9	100		7 704	100
Road transportation	326,4	82		4 385	57
Rail transportation	62,4	16		3 007	39
Water transportation	7,1	2		312	4

in a survey reported by Väätäinen, Anttila, Laitila, Nuutinen and Asikainen [29]. The condition and maintenance of the Finnish road network was found as one of the three most significant adverse factors by decreasing the cost-efficiency of the long-distance road transportation. The most important development objective found was the improvement of the road network condition and its maintenance. Road network condition and its impact on transportation was clear from the responses received in the study [29]. The decreasing trend in road network conditions hinders the use of bigger and heavier vehicles, and also increases the cost of transportation. The survey received 15 responses to the questionnaire sent out to 40 recipients. Together with the questionnaire responses additional material was gathered from the interviews of 10 representatives from the forest and transportation industry. Due to the small number of responses Väätäinen et al state that the results of the survey are only indicative and not statistically significant but still the results follow the same direction as the results from earlier studies and the common view of the transportation industry [29]. Also Holm, Hietala and Härmälä referred in [16] to the common view of the transportation industry on the poor condition of the road network shared by the road network specialists and

users.

The condition of a road, or the road network, is somewhat loosely defined concept. Different sources define the road condition differently or they do not give any clear definition what is included in it. The condition in relations to road (or road network) can be based on a combination of different factors. These factors can be in effect in long term, seasonally or in more temporal periods. Such factors can be different kind of restrictions (e.g. vehicle weight, width), situational (e.g. need of snowplowing, flooding), properties (e.g. condition of the road surface and/or structure) or even opinions (e.g. result from an opinion survey of different road user groups), or combination of the aforementioned. The definition for road condition used in this thesis is further discussed in Section 3.2.

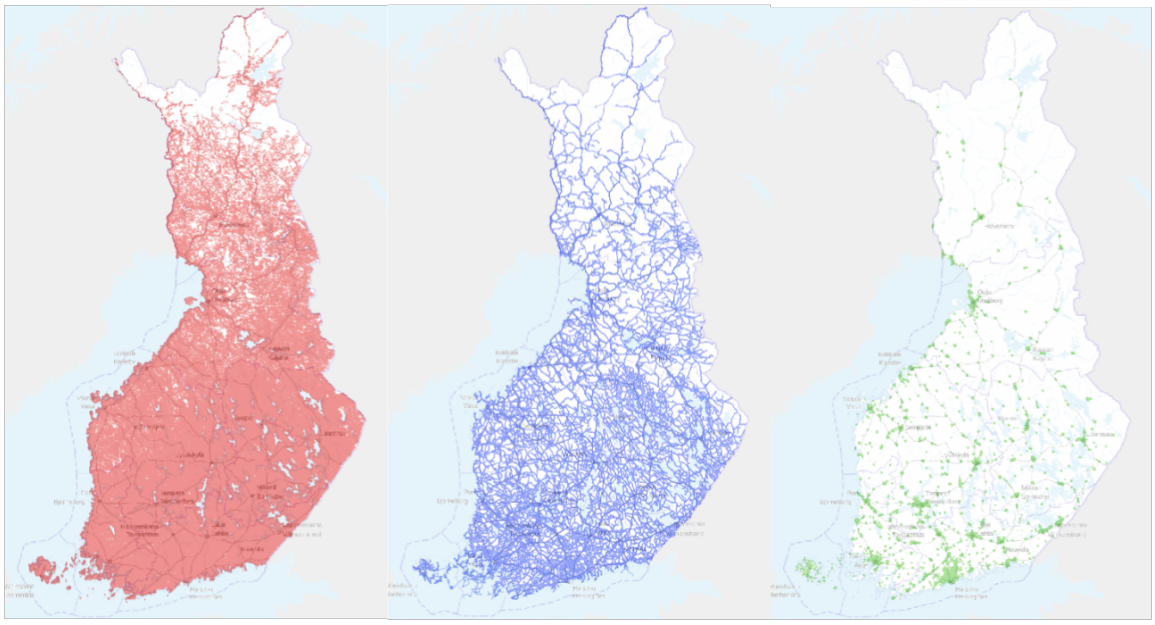

Figure 1.1: Finnish road network governance division according to the *Digiroad Database* [31]. **Left:** Private-owned roads. **Middle:** State-owned roads. **Right:** Municipality-owned roads.

The length of the Finnish road network is approximately 454 000 km and it consists of the public roads governed by the Finnish state, the public streets and roads governed by the municipalities of the Finnish state and the privately owned private and forest roads [32, 16]. The privately owned private and forest roads make the largest part of the total road network with 77 % and with the length of 350 000 km approximately. The length of the roads governed by the Finnish state is approximately 78 000 km (17 %) and the length of the roads governed by the municipalities of the Finnish state is approximately 26 000 km (6 %). The roads governed by the Finnish state are divided into main-volume roads (13 300 km) and low-volume roads (64 700km) in [16]. From here onwards the term lower road network is in thesis used to describe

the previously mentioned privately owned roads (private roads and forest roads) and the roads governed by the Finnish state municipalities. The density of the private, state and municipality governed roads are shown in Figure 1.1 [31].

The conditions of the lower road network has had an impact on the transportation costs of the natural resources industry and the costs of the transportation companies according to Holm et al [16]. The weight restricted bridges and sections of road forces to make changes to transportation route plans which result in longer routes and increased time of travel. The longer routes and the more time spent to travel have both increased the direct transportation costs. The roughness of the road surface was also considered as a factor in the transportation costs. The more rough road surface increases the time of travel and fuel consumption and therefore increases the costs. The impact of other types of cost on national or regional economy were not part of the estimation. If the weight restricted bridges and sections of road were repaired and the road conditions would be improved the combined transportation costs of forest and food industries together would roughly decrease by 5 %, and by 6,8 % alone in the forest industry [16]. With the rough estimate Holm et al estimated a decrease of 25 MEUR in the road transportation costs for the forest industry in 2012 and a 50 MEUR decrease in costs for the total industry in Finland. Using the same rough estimate by Holm et al on the 326,4 MEUR total cost of the road transportation in 2017 [28] gives an estimated 22 MEUR decrease in the road transportation costs for forest industry. The reduction in the estimated figures of the decrease in the road transportation costs between 2012 and 2018 is due to the decrease in the total road transportation costs. In [16] Holm et al point out that it was only possible to consider the main-volume and low-volume roads for the routes used to come up with the rough estimate and that the portion of the low-volume roads varied from 45-63%. The reason why the private and forest roads (77% of total road network) were not considered is not explained but one reason could be that the condition and restrictions information about the private and forest roads is not available.

In [33] Venäläinen, Alanne, Ovaskainen, Poikela, Strandström have estimated that the seasonal variety is causing approximately 70 MEUR costs alone for the domestic wood supply chain. The main cost factors were the cost of capital of the additional harvesting equipment (59 %), the decreasing value of wood due to seasonal stockpiling (13 %), the maintenance and snowplowing costs of the private roads (10 %) and the changes in long-distance transportation (8 %). Venäläinen et al have listed several means that could help to reduce the seasonal variety or the effects caused by it. The means that are interesting for this thesis are the need on information sources of timely information on weight restrictions and thaw damaged road sections, and the utilization of crowdsourcing as the means to collect timely information on road main-

tenance needs. These means give motivation in this thesis to analyze what kind of information is useful and can be collected with smartphone based crowdsourcing to help the transportation planning and the road maintenance needs.

Venäläinen, Räsänen and Hämäläinen have summarized in an earlier study report [34] that the most important information resource holding the Finnish street and road network data is the *Digiroad Database* administered by the Finnish Transportation Infrastructure Agency. While the *Digiroad Database* holds information about the private roads the available data was found to be very limited for the use of wood transportation stakeholders. The private road data additionally produced and stored by several different actors was found often to be incompatible with one another or not in electronic form. From the conclusions by Venäläinen et al in [34] it can be seen that timely data of long-term, seasonal and temporal period road condition factors is required for the use of the wood transportation stakeholders. The points in the action plan suggested by the study [34] that are interesting for this thesis are the results from the piloting of crowdsourcing as a data collection method for road network conditions data, and the development of data collection methods of the road network conditions. These points support the previously mentioned motivation for the analysis done in this thesis.

The modern day smartphone with rich variety of sensor capabilities, computing power and data sharing possibilities make it the obvious tool for collecting location based data as individual observations. The wide-spreadness of such smartphones make crowdsourcing as a data collection method feasible. Cloud computing platforms offer a convenient place to gather the crowdsourced data and process it into useful information to be shared. The Finnish Forest Centre has published a mobile application to crowdsource the road condition data of Finnish forest roads. The author of this thesis was part of the team that helped to develop the mobile application with the cloud-based backend system. The focus in this thesis is to find useful methods to automate the assesment of the forest road conditions by reviewing existing literature. Particularly the focus is in reviewing literature of useful computational methods, such as machine learning methods, to detect the types of road conditions based on the measurement data collected from the inertial sensors of a smartphone. In Chapter 2 the related prior work done which has partly led to writing this thesis are discussed. The Chapter 3 introduces the factors and the road anomalies that are considered when assessing the condition of the Finnish forest roads. In Chapter 4 the computational methods found to potentially detect the presented road anomalies to assess the road condition are reviewed. The Chapter 5 summarizes the use of the reviewed computational methods for the detection of the presented road anomalies. And finally the Chapter 6 concludes the work with on overview of this thesis.

2. Related prior work

In this chapter some of the closely related prior work that has partly led to write this thesis is discussed to provide the contextual setting. In Section 2.1 the *Data to Intelligence* research program and the concept pilots conducted under the *Forest Big Data* research area are introduced. The focus is in the most interesting results derived from the concept pilots. Section 2.2 briefly sums up the prior work done to develop a mobile application for smartphones to enable the crowdsourcing of the road conditions data. The literature review about the computational methods for detection of road anomalies done later in this thesis is aimed to be used to develop the aforementioned mobile application further.

2.1 Previous research programs and concept pilots

The aim of the *Data to Intelligence* (D2I) research program was to develop intelligent tools and methods for big data management based on the needs and the challenges faced in the different business sectors in Finland. *Forest Big Data* (FBD) was one of the research areas in the D2I program with stakeholders in the forest industry [34, 10]. The aim of the FDB was to improve the efficiency and the quality of the wood supply chain planning and operations. Additionally the aim was to improve the cost-efficiency by digitalization of the wood procurement process.

The study by Venäläinen et al was conducted in the FDB research area and it addressed the digitalization of the road network information to be utilized in the domestic wood transportation [34]. The study contains a status report on the state of the road network information and data production, results of the two pilots executed during the study and a vision statement together with a action plan for the contents, production and sharing of the lower road network conditions data. The vision includes a data platform to combine the different sources of the lower road network road related data, real-time data services for lower road network conditions data and a discussion forum to steer the production, distribution and the use of the lower road network data.

The most interesting action points from the vision statement regarding this thesis are the fusion of the different sources of permanent road network data, the development

of road network data collection methods and the results of piloting crowdsourcing of the road network conditions data with smartphones. In the pilot the smartphones were used to collect pictures and sensor data about the lower road network. The results from the pilot were seen as encouraging and showed the potential of the already existing solutions to be used to improve the production and distribution of the lower road network data [34].

Currently different kinds of data about the Finnish road network is stored by different stakeholders as mentioned earlier in the Chapter 1. Combining the different data sources under one platform and distributing from the platform onwards is useful for many use cases involving the authorities and companies [34]. The study [34] called such a hypothetical platform as *Forest Digiroads* and the work on the platform has since progressed by the *Finnish Forest Centre* under the name *YTPA* [21].

Crowdsourcing is seen as one of the important potential methods to collect the lower road network conditions data in comparison to the traditional road conditions data collection methods [34]. Conducting a road inventory by traditional means on lower road network is impossible in reasonable time in practice due to the vast size of the network. Also the lower road network does not have road weather stations to report the road weather conditions data automatically as is the case with the main-volume roads. The user groups of the lower road network seen as the potential crowdsourcing data collectors are forestry service providers, wood transports, dairy transports, school transports, carriage transports, postal deliveries, snowplowers and private car users [34]. It is easy to see how all of the mentioned user groups could benefit from the data to be collected but it is more difficult to see what are the incentives for each of the user groups to collect the data. Virtually everyone travelling the forest roads with a smartphone is a potential data collector but what is the interest for a such person to collect and share the data. By recognizing the potential user groups is good way to start to solve the problem by having figured out the groups with common interests. But how to then incentive the potential user groups to crowdsource the data is an interesting problem. However this problem is not discussed further in this thesis. Table 2.1 lists the requirements for the improvement of the lower road network and transportation data according to Venäläinen et al [34]. Considering the listed requirements for most of them crowdsourcing with smartphones seem like a valid option to collect timely information about them. Some of the requirements could be fulfilled with automated road anomaly detection in a smartphone and others would require manual input from the user. The road condition factors and road anomalies on the lower road network are further discussed in Chapter 3 and the computational detection methods in Chapter 4.

The goal in one of the pilots reported in the study [34] was to test and evaluate the images from the camera and the sensor data collected from a smartphone attached to

Table 2.1: Requirements to improve the lower road network and transportation data [34].

Permanent lower road network data	**Lower road network conditions**
The driveability and bearing of the forest roads at different times of the year	Information about the thaw restrictions on roads
The high ongitudinal slope of the forest roads	Information on the snowplowing and road melting actions
The differences of an actual forest road in comparison to forest road structural instructions and to the terms of the *Kemera* funding for private roads	Trafficability of the roads for transportation planning and road maintenance actions
Condition of the lower road network from maintenance improvement point of view	Locations and the type of turning points for vehicles on forest roads
The locations and weight restrictions of bridges on lower road network	Timely information about acute road anomalies
Locations of the approved on-loading and stockpiling sites for wood, the parking and switching places for trailers, the parking places for cranes on private and municipality owned land	Reachability of the on-loading and stockpiling sites in different weather conditions
The approved routes for heavy vehicles	Ongoing on-loading and passers-by on forest roads
Locations of the new forest roads and the plans for their locations	
Inventory and condition of the bridges and culverts on private roads	
Up-to-date contact information of the road administrators	

the a vehicle's windscreen. The images from the camera and the data from the sensors were collected with a smartphone app made in Technical University of Tampere. The data was collected with two different vehicles, with a wood transport vehicle and a passenger car. The collected data was evaluated for the use of automatic detection of potential road anomalies based on images from the camera, for locating the potential road anomalies based on the sensor data and for the usefulness for lower road network management and transportation planning. One of the conclusions from the pilot was that providing still images from the location of a road anomaly detected from the sensor data was providing useful information about the surroundings to the end users even if the anomaly itself was not detected from the images with computer vision methods. Regarding the use of computer vision it was recognized that there were several sources of problems causing poor-quality photos. For detecting line-based anomalies from a set of consecutive images a few poor-quality images does not make a difference. For detecting point-based anomalies from a single or small set of images, an improved auto-correction method for the quality of the images would be required. One other conclusion regarding the sensor data was that the use of heavy vehicle or driving on a gravel road decreases the reliability of the sensor data. Another conclusion regarding the sensor data was that collecting the data many times and with different devices increases the reliability analysis from the sensor data. The changes between the different observations for the same road sections are more useful in describing the conditions than a single observation. Venäläinen et al found that sensor data to be more reliable than the images in some situations like where the image analyse results in too good condition of the road. As a final conclusion in order to gain real benefits from the images and the sensor data the collecting should cover large area and be a frequently repeated process [34].

Venäläinen, Raatevaara, Pihlajisto, Melander, Hienonen, Hämäläinen and Strandström reported about more extensive pilot executed with a goal to develop the lower road network condition data crowdsourcing and to evaluate the data analyze methods for the needs of the road maintenance and wood transportation planning [35]. In the pilot 20 smartphones were used by attaching them into the windscreens of wood transportation and forest industry employees vehicles. The smartphones were installed with a mobile application purposely build to automatically collect video and sensor data (gyroscope, accelerometer), and send it to be analyzed centrally with computer vision and sensor data algorithms. In addition each vehicle was equipped with a wireless button which the driver could use to manually report the location, together with an audio message, of the observed road anomalies. The vibration of the road surface and the locally experienced swaying of the vehicle were inferred from the sensor data to be used to detect road anomalies. The road anomalies that were detectable with the help of the collected sensor data were thaw road damage, boulders, rutting, dips, holes, abnormal horizontal or longitudinal slope of the roads and rough road surface [35].

2.2 Mobile application for data crowdsourcing

In January 2019 the Finnish Forest Centre (FFC) published a mobile application to enable the crowdsourcing of road condition data of forest roads in Finland. The mobile application with a backend system was developed by RoadsML, a company co-founded by the author of this thesis [24]. The company spinned off from an hackathon challenge in spring 2018 hosted by the FFC as part of the Bioeconomy project (DataBio) [9].

To maximize the crowdsourcing potential to collect road conditions data the mobile application was made available to all users with a Android platform smartphone as free of charge. The application has a simple user interface and it is easy to use. The mobile application makes it possible to collect the location points and the accelerometer measurements of the traversed route, accompanied with the users perception on the condition of the traversed route. With the mobile application it is also possible to collect the observation type and the location point of user reported observations. Currently all the data has to be collected, in a way, manually by the user with the help of the mobile application's functions. After enough data is collected the expectation is to make it possible to automate some of the user generated detections in the mobile application with the help of suitable computational methods (which is the motivation for the literature review in this thesis).

The data from all of the mobile applications is collected to a dedicated data storage hosted on a cloud computing platform. The Finnish street and road network data

is provided from the *Digiroad Database* as an open data source and stored into same dedicated data storage together with the crowdsourced mobile application data. In the cloud computing platform the crowdsourced data regarding the routes are matched with the *Digiroad Database* data. The crowdsourced accelerometer data and the user's perception of the route are processed as a result of the condition of the matching road sections. The crowdsourced observation points from the route are also matched and mapped with the road sections. Both the road conditions and the mapped observations of the road sections are accessible to FFC which they have used and published in a web map service called the *Metsätietieto* [22].

The solution architecture for the mobile application and backend system is in alignment with the vision for forest road data stated in [34]. The data about the lower road network is collected by means that enable the data to be crowdsourced from the road users. The collected data is related to the *Digiroad Database* data model which is envisioned as the underlying data model for the platform (*Forest Digiroads*) to collect and combine all the different data sources [34, 21]. The collected data can be sourced to a more common platform for forest road network data when such a platform (*YTPA*) comes available. The role of such a platform is currently acted by the FFC *Metsätietieto* web map service.

3. Identifying the road conditions

This chapter further discusses some of the practicalities in identifying the road conditions. In this thesis the motivation is to find computational methods that utilize the smartphone sensing capabilities to detect the road anomalies to further assess the road conditions. More precisely the focus is in Android platform smartphone capabilities with its inertial sensors. The image and video capabilities with computer vision are not discussed in this thesis for the reason that the utilization of such capabilities limit the orientation and placement of the smartphone in the vehicle. The Section 3.1 discusses some of the practicalities with smartphone inertial sensing. With inertial sensors the accelerations and the changes in the orientation of the smartphone can be measured and used to infer the different road anomalies based on their characteristics reflected in the measurements. With location information from the smartphone location services the measurements can be related a place. For example with location information the collected data can be related to the road sections in the *Digiroad Database* data model as briefly discussed in previous Section 2.2. Finding a location and relating the location with other location information are not further discussed in this thesis as they are easily solved with location services and spatial databases. The Section 3.2 discusses further the evaluation of forest road conditions. The detection of road anomalies and how they are assumed to reflect in the inertial sensor measurements are discussed in the subsections. These assumptions are made to help to identify the relevant recent literature about the use of computational methods, such as machine learning, for the automated road anomaly detection.

3.1 Practicalities in sensing the road conditions

Any modern day smartphone contains a number of sensors to provide information on its location, movement and the surrounding environment. Inertial sensors are hardware components embedded in the smartphone. Inertial sensors are commonly known as the accelerometer sensor and the gyroscope sensor. The accelerometer measures the acceleration forces and the gyroscope measures the angular velocities on three orthogonal axes respectively. Depending on the manufacturer of the device a smartphone may in-

clude a varying number of other device or software sensors like barometer, geomagnetic field, gravity and thermometer for example.

3.1.1 About sensors and coordinate frames

On the Android platform the sensors embedded in the device are divided into three categories: motion, environment and position [14]. Motion sensors measure the acceleration and rotational forces, and the category includes accelerometers, gravity sensors, gyroscopes, and rotational vector sensors. Environment sensors measure different environmental properties such as illumination and pressure amongst others. The environment sensor category includes barometers, photometers and thermometers. Position sensors on Android platform measure the device's physical position (excluding location), and the category includes orientation sensors and magnetometers. The sensors currently supported by the Android platform are hardware-based (accelerometer, gyroscope, light, magnetic field, pressure, proximity, humidity, temperature) or software-based (gravity, linear acceleration, orientation, rotation vector) where the software-based sensors derive their measurements from one or two of the hardware-based sensors. Some of the sensors can be either hardware or software based (gravity, linear acceleration, rotation vector). The sensors and their measurements are accessed by using Android sensor framework. Any one device does not need to have embedded all the sensors supported by Android sensor framework and a device can have more than one same type of sensors. The device location through a GNSS receiver data is not part of the Android sensor framework but is rather accessed thru Google Play services location API. From the location API apart from the evident location information of the device also the velocity information of the device can be obtained.

The sensor data values from the Android sensor framework are expressed in a standard 3-axis coordinate frame [14]. Accelerometer, gravity sensor, gyroscope and geomagnetic field sensor use a coordinate frame that is relative to the device screen when the device is held in its default orientation. The default orientation depends on the device and it can be either portrait or landscape. In the default orientation the x-axis is horizontal (lateral), y-axis is vertical and z-axis (longitudinal) points directly out from the screen. Figure 3.1a illustrates the coordinate frame used by the device sensors in default orientation (portrait). Figure 3.1b illustrates the coordinate frame of the vehicle. From here onwards in this thesis the lower case triad $\{x, y, z\}$ is used to refer to the device coordinate frame axes and upper case triad $\{X, Y, Z\}$ is used to refer to the vehicle coordinate frame axes. The easiest method to align the two coordinate frames is to attach the device securely in the vehicle aligned with the vehicle's coordinate frame. The different road anomalies, as they are experienced by the

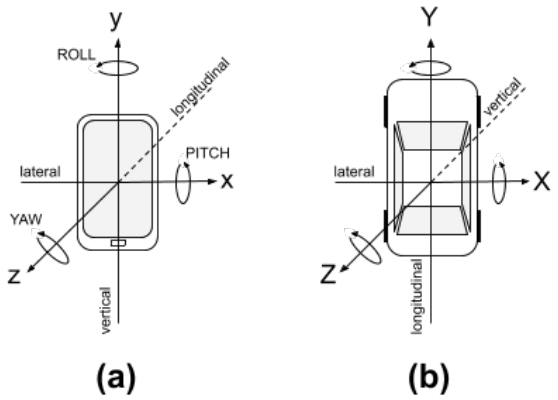

Figure 3.1: Coordinate frames. (a) Used by the sensors. (b) Used to reference a vehicle movement.

vehicle, can then be detected from the similarly aligned axes of the device. Even with careful placement of the device in the vehicle easily results in the coordinate frames not being perfectly aligned and thus effecting the measurements of force on each axis. The difference between the coordinate frame alignments can be compensated for example with the help of angular velocities from the gyroscope if the coordinate frame of the vehicle is known or can be discovered with the help of other sensors in the device. The alignment of the device's coordinate frame axes can be reoriented to the closest axes of the vehicle's coordinate frame as long as the parallel axes are known in order to do the detection of a road anomaly from correct axis data. Similarly the compensation then needs to be done to the same closest axes to minimize the error in compensation. The changes of the acceleration forces and angular velocities on the device coordinate frame axes are observed to detect the road anomalies experienced by the vehicle to help to infer the condition of a road on the lower road network. As an example of the differing coordinate frame alignments the Figure 3.2b illustrates the coordinate frame of the vehicle and the Figure 3.2c illustrates the orientation of the device and its coordinate frame in the vehicle in Figure 3.2a.

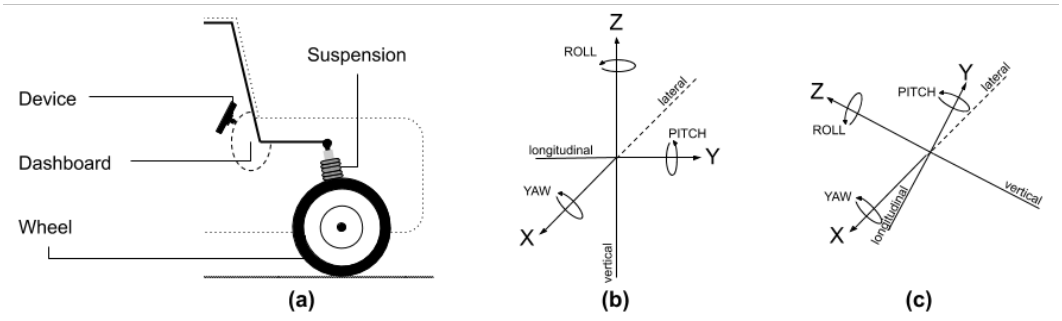

Figure 3.2: Device placement and vehicle characteristics. (a) Secure holder attachment. (b) Coordinate frame orientation of the vehicle on left. (c) Coordinate frame orientation of the device in the vehicle on left.

3.1.2 Device placement and vehicle characteristics

The device placement in a moving vehicle is understandably a key factor in obtaining good quality measurement data about the road from the inertial sensors. If the device is placed loosely inside the vehicle the inertial sensor measurement data is subjected to unwanted noise which effectively complicate the detection of the road anomalies. Loose placement of the device allows the device to move erratically during the vehicle movement and thus affect the the collected inertial sensor measurements. Examples of loose placements of the device are such as resting freely on the dashboard, on the passenger or on the back seat. Also placing the device in a cup holder, the glove or a door compartment or similar will allow the device to move and potentially generate excess vibrations to the measurement data when colliding with the sidewalls of the compartment.

With intuition the optimal placement of the device in the vehicle is with a secure holder which is attached as close as possible to the vehicle chassis. The secure holder prevents the free movement of the device during vehicle movement. Adjustable secure holder also makes it possible to align the coordinate frame of the device approximately to the alignment of the coordinate frame of the vehicle. By attaching the device in a secure holder to as close to the vehicle chassis (windscreen, dashboard) as possible is a practical way to remove as many dampening factors as possible between the device and the road surface. Figure 3.2a illustrates a rough example of the mechanics of a device placement with a secure holder attached close to a vehicle chassis. The holder holding the device is attached to the dashboard of the vehicle with the dashboard attached to the vehicle chassis. The wheel of the vehicle is attached to the vehicle chassis with a suspension and dampening system. Roughly speaking the wheels collect and transfer the vibrations of different amplitudes and the elevations from the road surface through the picture-like mechanics (Fig. 3.2a) of the vehicle all the way to the attached device. The device's inertial sensors measure the transmitted acceleration forces and angular velocities caused by the road surface and provide the measurements for the use of applications. In between the device and the road surface there are many potential sources that affect the vibrations experienced from the road surface when measured by the device. The structure of the tire and the tire air pressure of the wheels are one of the factors that affect the vibrations from the road surface. Suspension system and the shock dampeners are also affecting the vibrations as they are transmitted from the wheel. Depending on the material of the dashboard the vibrations transmitted from the vehicle body are diluted even more. Therefore a secure holder with a device attached to the windscreen of the vehicle would intuitively thinking be better choice than the dashboard to measure the vibrations. The windscreen is more solid and

therefore affects the vibrations less than the dashboard. The type and material of the secure holder also affect the amplitude of the vibrations. Apart from the mechanics also the weight of the vehicle affects the vibrations from the road surface. With heavier vehicles, like wood-trucks, the weight suppresses the possibility to generate some of the vibrations collected from the road surface. Specialized vehicles like wood-trucks may also have special air suspension systems and tyre pressure control systems that suppress the collected vibrations.

Some of the other common vehicle characteristics are the axel width and wheel footprint. The axel width determines how far apart the footprints of the wheels are. Depending on the axel width the vehicle may not fit well to the rutting formed to road surface. This makes the detection of rutting more likely. The footprints are effectively the area from which some of the road anomalies can be detected. The detectable area is relatively small when comparing the size of the wheel footprint to the area for the road. Therefore only a small portion for the total road width is under detection at one drive. Additionally the driving lines are chosen by driver of the vehicle which ultimately dictate which road anomalies are detected.

3.2 Road condition factors

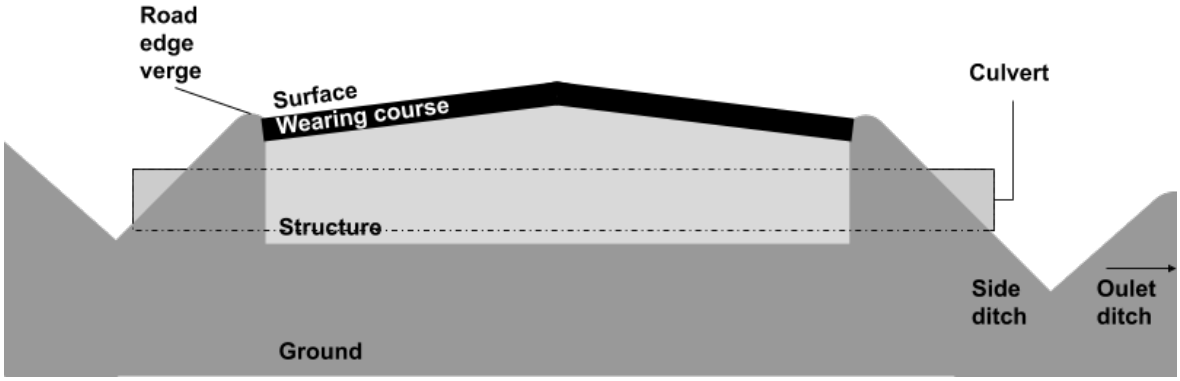

Figure 3.3: Forest road crosscut.

This section discusses the road anomalies which are considered when assessing the factors of the forest road conditions. The main reference used in this thesis to identify such factors and road anomalies is the project report [18] done by Antti Korpilahti. The project produced instructions for visual inspection to help to evaluate the condition of the forest roads and defined a 3-class classification system to classify the forest roads based on the evaluation. A rough sketch of a crosscut of a forest road is illustrated in Figure 3.3. The condition of a forest road is evaluated based on the factors described in Table 3.1. The condition factors are divided into two groups: road structural condition

Table 3.1: Factors used to evaluate a forest road condition in Finland [18].

Structural condition factors	1 - Bearing deficiencies	Sections of road structure thaw Sections of road surface thaw Weak (soft) soil
	2 - Structural deficiencies	Flat road structure Deficit in road structure
	3 - Dewatering	Side and outlet ditches Culverts
	4 - Wearing course	Thickness Quality
	5 - Boulders	
	6 - Road geometry and dimension	Rectifiable bends Steep slopes Poor sight distance Insufficient meeting points Insufficient turning places
	7 - Brushwood	
	8 - Bridges	Condition Restrictions
Surface condition factors	9 - Road surface	Surface uniformity (trails, potholes, boulders, road edge verges, lateral slope)

factors and road surface condition factors. Each factor is evaluated based on the instructions given in the project report and classified into one of the three classes: good (3), average (2) and bad (1). The road bearing is classified by two damage classes: road body thaw and road surface thaw. The other road condition factors are classified by condition classes. The general description for the three road condition classes are described in Table 3.2.

In the following subsections each of the factors, including the possible road anomalies contributing to a factor, are first presented and then discussed whether they could be detected from the inertial sensor measurements. The basic assumption in the following discussion is that the road anomalies are experienced with a moving vehicle and the impact with the road anomaly is generating some excessive forces that are measured with a smartphone inertial sensors. The changes in the acceleration forces are assumed to be detectable from the accelerometer sensor measurements and the changes of angular velocities from the gyroscope sensor measurements. It is further assumed

Table 3.2: General forest road condition classification classes in Finland.[18].

Good (3)	Condition is good. Occasional wear can be expected. Only basic road maintenance is required. No additional repairs or renovation is required. Expected service level is fulfilled.
Average (2)	Condition is average. Additional follow-up on repairs and some individual repair work is needed. No immediate renovation is required. Expected service level is still satisfied.
Bad (1)	Condition requires improvement. Repairs and renovation are required and is worth to do in this class. Immediate need of repairs. Expected service level is not fulfilled.

that the smartphone is securely attached to the vehicle (windscreen, dashboard) and aligned with the vehicle coordinate frame when the inertial sensor measurement data is collected to help to describe the correct axes to observe the road anomalies.

3.2.1 Road bearing and structural deficiencies

According to Korpilahti the road bearing and structural deficiencies (Tab. 3.1) are best observed during the period of spring thaw when the ground contains a lot of water due to the melted snow and ice [18]. Bearing and structural deficiencies of the road sections are evaluated based on the visually observable road structure and road surface thaw.

Table 3.3: Damage classes for road structure thaw [18].

3	Moderate softness of the road structure. Road edge collapses may be found. Majority of the road is supporting. Moderate deceleration of speed.
2	Soft spots due to water pushing through the surface. Driving lines need to be adjusted. Considerable deceleration of speed.
1	The structure of road is badly mixed up. The floor of a passenger car may contact the road. Driving line needs to be considered carefully. The driver has to stop and consider whether it is possible to pass the damaged spot.

Table 3.4: Damage classes for road surface thaw [18].

3	Moderate softness of the road surface. Moderate deceleration of speed.
2	Visible softness of the road surface. Driving lines need to be adjusted. Considerable deceleration of speed.
1	The road surface has totally softened. Rutting have formed on the driving line. Driving line needs to be considered carefully. Considerable deceleration of speed.

Based on the damage class descriptions in Table 3.3 and Table 3.4 both the road structure thaw and the road surface thaw causes different level of softness of the road and occasional collapsed road structure as road anomalies. The result from the softness of the road is observed as the deceleration of speed of the vehicle. The assumption here is that the speed deceleration events caused by the different levels of softness of the road would generate different levels of changes in acceleration force along the vehicle's Y-axis. The deceleration of speed and changes in average speed could also be detected by using the Google Play services location API. The occasional collapses of the road structure are observed as changes in orientation of the vehicle. The changes in the orientation of the vehicle are assumed to cause changes in the angular velocities

mainly along the Y and X axes. Also the collapses of road structure are assumed to cause changes in the acceleration force on Z-axis. The driving line adjustments and swerving from driving in rutting are also observed as changes in orientation of the vehicle from a smaller scale of swerving. These changes in orientation of the vehicle are assumed to cause changes in the angular velocity along the Z-axis. Also changes in the acceleration forces along the X and Y axes based on the orientation changes are assumed. It is assumed that a combination of detected changes in speed and in orientation could be used to indicate the possibility of thaw on a scale from 1 to 3 to conform the damage classes in general. Differentiating between road structure thaw and road surface thaw is assumed to be more difficult. As a reference also Venäläinen et al reported the use case of detecting certain level of thaw with the help of accelerometer measurements [34].

3.2.2 Dewatering

Functioning dewatering has a significant impact on the condition of a forest road [18]. The observables that require inspection include the condition and functionality of the side and outlet ditches, and culverts. Blockages in ditches and culverts confines the water from flowing away from the road structures. Still water keeps the road structures wet which then contributes to probability of thaw damage and softness of the roads. During winter the water freezes which potentially causes frozen road damage. The frosting and melting of the water pockets in road structures may potentially either raise or lower the insecurely installed culverts which in turn causes bumps or potholes on the forest road.

Based on the condition class descriptions for ditches in Table 3.5 and for culverts in Table 3.6 the detection of the deficiencies in side and outlet ditches or damage in

Table 3.5: Condition classes for side and outlet ditches [18].

Good (3)	Side and outlet ditches exist and are well functioning. There are no blockages keeping the water from flowing.
Average (2)	Side and outlet ditches exist at minimum under the places important for the dewatering of the road structures. Ditches are functioning adequately during heavy water flow. Some blockages might exist which are keeping the water from flowing during light water flow.
Bad (1)	Side and outlet ditches are missing under the places important for the dewatering of the road. Side and outlet ditches are blocked or they contain such obstructions that keep the water from flowing. Dewatering does not work.

Table 3.6: Condition classes for culverts [18].

Good (3)	Culvert is new or similarly in good condition. Damage that does not affect the functionality of the culvert may exist. Side and outlet ditches exist and are well functioning.
Average (2)	Damage that does not prevent the functioning of the culvert under normal circumstances can exist. Functionality of the culvert under normal circumstances is adequate.
Bad (1)	Culvert has significant damage. The functionality of the culvert is poor under all circumstances.

culverts from a moving vehicle directly with inertial sensors of the device is not possible. Assumption here is that the softness of the road is detected based on the same principle as previously discussed with thaw damage in Section 3.2.1. It is further assumed that it is not possible to infer the cause (thaw vs. blocked ditch or culvert) of the detected softness of road. Additionally the deficiencies in ditches and in culverts may result in road anomalies like bumps and potholes. Bumps or potholes are road anomalies that are observed as a sharp rising or a falling of the vehicle when experiencing a bump or pothole with its wheels. The assumption is that a rising or a falling is causing a change in the acceleration force mainly along the Z-axis. It is also assumed that a rising or a falling cause a change also in the angular velocities mainly along the X and Y axes. The characteristics of a bump and a pothole are assumed to be separately detectable as a bump (rising) or a pothole (falling) from the sensor data measurements. The detection of a bump or pothole could be used as indicative information to suggest the possibility of a dewatering problem.

3.2.3 Wearing course

The condition of the wearing course of a forest road is assessed by visually observing the thickness and the quality of the wearing course [18]. The wearing course has to be at least 5 cm thick and the recommended main particle size of the material is 0 - 16 mm or 16 - 32 mm. The material can be either crushed bedrock, crushed gravel, natural gravel or crushed moraine. The solidness of the wearing course is based on the mixture of required size main particles of the given material and more finer grained gravel or sand which is used to tie the particles together. The mixture of the materials need to be of appropriate proportions to form a good solid wearing course. With less main particles and more finer grain gravel or sand results in loose and soft wearing course. With more main particles and less or no finer grain gravel or sand results in loose and rough wearing course.

Table 3.7: Condition classes for the wearing course [18].

Good (3)	Thickness of the wearing course is adequate and the quality of the material is good. The surface of the wearing course is uniform and solid.
Average (2)	Thickness of the wearing course is too thin or the quality of the material is too fine or rough, which is slowing down the vehicle speed.
Bad (1)	The wearing course has worn off, the material is too fine or rough, which is causing problems for movement.

Based on the condition class descriptions in Table 3.7 the wearing course deficiencies could partly be detected from the inertial sensor measurements of the device. Assuming the wearing course material would cause vibration to vehicle at different scales (amplitude, frequency) based on the solidness and the particle size. Such vibrations are assumed to cause constantly variating acceleration force of different scales depending on the wearing course material used, thickness and condition mainly along the Z-axis. Assuming further, the trembling also causes constantly variating angular velocities of different scales along the X and Y axes. The exact thickness of the wearing course is assumed to be more problematic to detect from the inertial sensor measurements but it is assumed that the thickness affects the scale of the experienced vibrations. Assuming the constant variation is lower the more thicker the wearing course is and more higher the more thinner the wearing course is. Deceleration of speed of the vehicle when the vehicle moves from better quality wearing course to more rough wearing course is assumed to be detected based on the same principle as previously discussed with thaw damage in Section 3.2.1.

3.2.4 Boulders, road geometry and dimensions

According to Korpilahti [18] the condition classification is not used when assessing forest road condition for the existence of boulders, the road geometry and dimensioning. Any road anomalies observed while inspecting the forest roads are simply recorded whether they exist or not. Boulders that break the surface of the forest road are observed as road anomalies. Assuming when a wheel is driven over a boulder it would generate changes in acceleration force and in angular velocities similarly as with bumps described in Section 3.2.2. All unsafe bends are observed as road anomalies. An unsafe bend is a bend where the turn is too steep in relations to the speed limit of the road [18]. When driving through an unsafe bend the assumption is that the turning of a vehicle is causing changes in the angular velocities mainly along the Z-axis. Driving though a bend with high enough velocity it is also assumed to cause changes also in the acceleration force along the X and Y axes. The change in speed of the vehicle is observed similarly as

described earlier in Section 3.2.1. The longitudinal slope is normally max 10 % and max 12 % on short distance, and any excessive longitudinal slope is observed as a road anomaly [18]. When driving along a forest road the assumption is that the changes in longitudinal slope of the road are causing changes in the angular velocity mainly along the X-axis.

3.2.5 Brushwood

Thick brushwood can prevent the proper functioning of the dewatering by blocking the side and outlet ditches [18]. Outgrown brushwood can also narrow down the driving lanes of roads effecting the mobility of the vehicles along the road.

Table 3.8: Condition classes for brushwood [18].

Good (3)	Only little brushwood on the side of the road or in side ditches. Brushwood does not produce a blockage for the forest road dewatering or the sight. Brushwood can be removed during ordinary maintenance. Diameter of brushwood is less than 2 cm.
Average (2)	Brushwood on the side of the road or in the side ditches is slowing down the dewatering of the forest road and is in the line of sight especially during summer. The brushwood has not been unrooted in several years. Brushwood can be removed during ordinary maintenance. Diameter of brushwood is less than 5 cm.
Bad (1)	The side of the road and the side ditches are completely covered by brushwood. The brushwood produces a blockage the effectively prevents dewatering. Brushwood narrows down driving lanes and is in the line of sight. Brushwood can be so thick that it cannot be removed during ordinary maintenance. Diameter of brushwood is over 5 cm.

Based on the description of the condition classes for brushwood in Table 3.8 the detection of a brushwood deficiency is not directly possible from with the inertial sensors of the device. Instead the brushwood deficiencies result in detectable road anomalies like softness of the forest roads and blocking of the driving lanes. Brushwood can cause blockages in side ditches which in turn can result in similar detectable road anomalies as discussed previously with the bearing deficiencies in Section 3.2.1 and with the dewatering deficiencies in Section 3.2.2. The blockages of the driving lanes are assumed to be detected similarly like the detection of bends in Section 3.2.4 with less speed or similarly like the detection of rutting in Section 3.2.1 with larger scale of swerving. Assumption is that by detecting softness of road together with the detection of turns or swerving as evasive steering events are used to indirectly suggest the existence of brushwood deficiency.

3.2.6 Bridges

The condition of a bridge is assessed by evaluating the wearing course and the structure of the bridge [18]. The wearing course is evaluated based on the damage and purity of the surface. The structure of a bridge is evaluated based on the visible damage. Bridges are usually constructed from steel, steel-concrete or wood.

Table 3.9: Condition classes for bridges [18].

Good (3)	Bridge is new or in similar condition. Condition is good, some normal wear and ageing can be expected. Some main structural elements can be adequate condition.
Average (2)	Deterioration and rusting damage that does not require immediate repairs. Some main structural elements can be in bad condition.
Bad (1)	Bridge has several damages that require repair, individual serious damage, full renovation is required or bridge needs to be replaced. Condition is unacceptable.

Based on the description of the condition classes in Table 3.9 the condition of a bridge is possible to some extent be evaluated from the inertial sensor measurements. If the location of a bridge is known (e.g. in the *Digiroad Database*) then the assessed condition of the wearing course can be related to that bridge. With by knowing that the collected measurements are from a bridge instead of road on ground could be considered in the condition evaluation. The assumption is that the condition of the wearing course on the bridge is detected from the inertial sensor measurements similarly as the roughness of the wearing course described in Section 3.2.3. Similarly as with the exact thickness of the wearing course the structural damage of a bridge is problematic to detect from the inertial sensor measurements. Assumption is that when driving over a bridge the materials used in the structure of the bridge could result in distinct vibrations. The main structure material is assumed to be detectable based on the distinct vibrations from the inertial sensor measurements and used help the evaluation of the bridge structure condition.

3.2.7 Road surface

According to Korpilahti [18] the condition of the road surface is assessed mainly based on uniformity of the surface. The assessment considers rutting, potholes, boulders, edge verges and the lateral slope of a road. The lateral slope of the road should be 5 % to ensure adequate dewatering from the surface of a forest road.

Based on the description of the condition classes in Table 3.10 the road surface condition is assessed by detecting rutting, dips, potholes, boulders, lateral slope of

Table 3.10: Condition classes for forest road surface [18].

Good (3)	Road surface seems to be in good condition and surface is uniform. There are no damages or the damages are almost undetectable by visual inspection. No anomalies exist that would disturb the driving comfort and no fear of damaging the vehicle. Dewatering from the road surface is good. The condition does not cause drawbacks to transportation or to daily traffic.
Average (2)	Some wearing and damages of the surface are visible. Some disturbances lowers the driving comfort. Deceleration of speed if required at times. Risk to damage the vehicle exists. Some dips, rutting and road edge verges exist. The condition does not cause drawbacks to transportation or to daily traffic.
Bad (1)	Wearing and damages are clearly visible, bad condition of the surface is obvious. Many disturbances lower the driving comfort. Deceleration of speed is experienced constantly and the driving line needs to be changed to prevent vehicle damage. Dips, rutting and road edge verges exist and dewatering of the road surface is not functioning. The condition causes drawbacks to transportation or to daily traffic.

road and road edge verges from the inertial sensor measurements. For detecting dips, potholes and boulders the same assumption applies here as previously discussed in Section 3.2.2 with bump and pothole road anomalies and with boulders in Section 3.2.4. The uniformity of the road surface is assumed to be detected similarly as the solidness of the wearing course described in Section 3.2.3. The rutting and road edge verges are assumed to be detected similarly as in Section 3.2.1 with rutting during thaw damage. With road edges the swerving effect is assumed to be more emphasised from one-side (right) along the X-axis. The road edge verges are assumed to be very hard to detect in practice since they are not on the normal driving driving path. The lateral slope changes of the road are assumed to cause changes in the angular velocity mainly along the Y-axis. Also the changes in the lateral slope of the road are assumed to cause changes in the acceleration force on the Z and Y axes.

4. Computational methods for road condition assessment

In this chapter the key findings in some of the relevant and recently published literature describing the different computational methods for assessing the road conditions with a smartphone inertial sensors are presented. As previously mentioned in Chapter 3 the focus is such literature work which makes use of the inertial sensor measurements in the detection of the different road anomalies discussed in Section 3.2. Most of the road anomalies previously discussed in this thesis seem to affect the acceleration forces and the angular velocities in a similar manner. The assumption nevertheless is that the different road anomalies generate some typical characteristics to the inertial sensor measurement data based on which the anomalies can be independently detected. The sections in this chapter are divided as follows. The threshold-based road anomaly detection methods are discussed in Section 4.1. Classification of road anomalies with different variations with Support Vector Machine is discussed in Section 4.2. In Section 4.3 methods used for detecting road roughness are discussed. Methods for detecting driving maneuvers are discussed in Section 4.4. A method for detecting accurately the vehicle speed is discussed in Section 4.5. And finally the methods for detecting bridge condition are discussed in Section 4.6. To help to compare the differences in the approaches taken with the different detection methods each of the sections are further divided into subsections discussing the collecting and preprocessing of data, the anomaly detection methods used and the evaluation results of each detection method. Summary of the computational methods for the detection of the road anomalies is presented in this chapter is discussed in Section 5.1.

4.1 Road anomaly detection

In this section the threshold-based anomaly detection methods of road anomalies are discussed. In the article [11] Eriksson, Girod, Hull, Newton, Madden and Balakrishnan describe the *Pothole Patrol* system (P^2) for assessing the road surface conditions. The system applies mobile sensing to detect and to report on the road surface conditions.

In the P^2 system a dedicated mobile computing unit, called the *pothole detector*, in each of the selected vehicles are used to collect and to filter the collected accelerometer data from the traversed road segments and to send the filtered detection data to the central unit [11]. The central unit stores the received detection data and uses location based minimum clustering to filter out the spurious detections. For the P^2 system a *loosely labelled* dataset extension is used to improve the detection accuracy. Based on many of the articles referenced in this thesis the P^2 system can considered as the pioneer solution for the threshold-based anomaly detection methods.

Based on the P^2 system Mohan, Padmanabhan and Ramjee developed the *Nericell* system in which a slight change for the threshold-based anomaly detection approach has been implemented [23]. Additionally the *Nericell* system implements the *virtual reorientation* in which Euler angles are used to align the device coordinate frame with the vehicle coordinate frame without the use of the gyroscope.

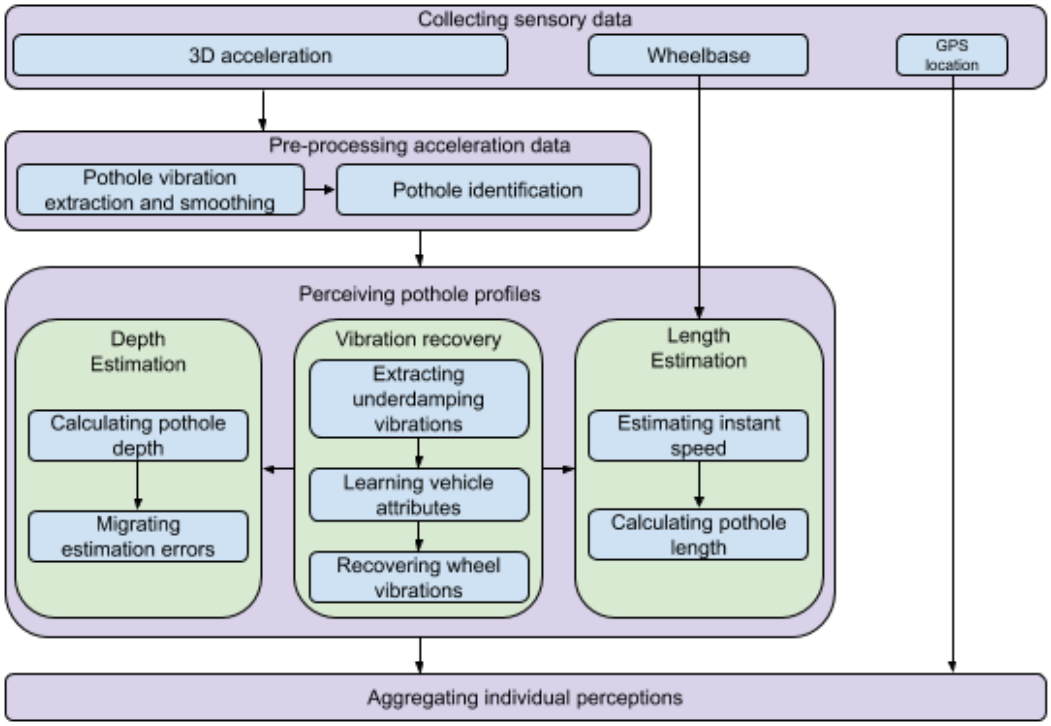

Figure 4.1: The system architecture of P^3 [37].

The *Perceiving Pothole Profiles* (P^3) system proposed by Xue G., Zhu H., Hu Z., Yu J., Zhu Y. and Luo, Y. similarly uses the threshold-based anomaly detection approach used in the P^2 system to detect road anomalies such as potholes [37]. When compared to the P^2 system additional preprocessing step and the *active vibration recovery* step to infer the accurate profile of a pothole are introduced with the P^3 system. Similarly to the P^2 system a data center approach is used to aggregate the detection results and to improve the perceived pothole profiles. The four layers of the

P^3 system architecture, illustrated in Figure 4.1, are discussed in the following sections.

Mednis, Strazdins, Zviedris, Kanoris and Salovo introduced a set of four different algorithms to detect potholes in [20]. The algorithms can be used in similar setting as the threshold-based anomaly detection approach used in the P^2, *Nericell* and P^3 systems. The algorithms were designed to be used in real-time detection applications in Android platform smartphones.

4.1.1 Collecting and preprocessing the raw data

For the P^2 system a set of training data was collected by repeatedly driving through several known segments of roads and recording the accelerometer measurements and exact location of the roads [11]. Each road anomaly observed was hand-labelled as a specific road anomaly type in real-time during the drive. In the post-processing of the collected data only significant detections were maintained to eliminate inaccurate hand-labelling. Seven different road anomaly types were used in labelling: smooth road, crosswalk/expansion joint, railroad crossing, pothole, manhole, hard stop and turn. The sections of road with no anomalies were labelled as smooth road. The frequencies of the anomalies in the collected training data set did not represent the true frequency of such anomalies in practice according to Eriksson et al [11]. A single *pothole detector* used in the P^2 system contained an embedded computer with Linux, external GPS (1 Hz) receiver and an external 3-axis accelerometer (380 Hz). To experiment with the implementation of the P^2 system seven taxi cars were mounted with a *pothole detector* to collect data in the Boston area. The components of a *pothole detector* were identically placed in the taxi cars: GPS receiver mounted on the roof of the car and the 3-axis accelerometer sensor to the dashboard inside the glove department and with the same orientation as aligned to the vehicle's coordinate frame. The two raw data streams (accelerometer, GPS) were combined in the *pothole detector* using linear interpolation between the GPS location points at the time of the accelerometer readings. The resulting combined data stream contained time, location, speed and heading from the GPS and 3-axis acceleration vector from the accelerometer. According to Eriksson et al the amount and coverage of the manually collected hand-labelled data was found too limited for training [11]. The manually collected data contained too many potholes which resulted in the *pothole detector* to over-report potholes (false-positives) when new data was processed. To overcome this problem additional traces of *loosely labelled* data was used to compensate the training data. The traces of *loosely labelled* data contained a known distribution of road anomalies without their locations. The extended training data was used to improve the detection performance of the detector.

Unlike the *pothole detector* in the P^2 system a smartphone ecosystem (Windows

Mobile) with a variety of sensing capabilities was employed in the *Nericell* system [23]. The implementation was experimented on smartphone devices with different setup of the sensing capabilities. The accelerometers (310 Hz) used in the experiment were external devices apart from the smartphone devices. The fact that *Nericell* was implemented on a smartphone ecosystem an interesting point for this thesis as it proves that such a detector can be build for smartphones. In the *Nericell* system an interesting aspect of the *virtual reorientation* was implemented, which is the key difference in comparison to the P^2 system. The *virtual reorientation* in the *Nericell* system is based on the accelerometer where as nowadays the reorientation is made less complex with the help of the gyroscope. According to Mohan et al with a disoriented accelerometer the road anomaly detection is more difficult to infer than with a well-oriented accelerometer [23]. The problem of a disoriented accelerometer is compensated with the *virtual reorientation* by virtually reorienting the accelerometer coordinate frame. For the *virtual reorientation* the coordinate frames for the device and for the vehicle are described similarly as in Section 3.1.1 with the slight difference in the coordinate frame's orientations. For the device's accelerometer a 3-dimensional Cartesian frame of reference is defined as orthogonal axes x, y and z. Also for the vehicle that carries the device a 3-dimensional Cartesian frame of reference is defined as orthogonal axes X, Y and Z. In the vehicle frame of reference the X-axis is pointing to the front, the Y-axis is pointing to the right and the Z-axis is pointing to ground. Accelerometer is said to be well-oriented when the frame of reference of the accelerometer (x, y, z) is aligned with the frame of reference of the vehicle (X, Y, Z). Otherwise accelerometer is said to be disoriented. The values of the axes from the accelerometer are denoted with a_x, a_y and a_z, and the values of the axes for the vehicle are denoted with a_X, a_Y and a_Z respectively. The *virtual reorientation* is based on Euler angles for which the Euler's theorem states that any rotation can be specified with three angles [23]. Mohan et al defines that any arbitrary orientation of the accelerometer (x, y, z) is achieved from the ground-truth orientation of the vehicle (X, Y, Z) with three consecutive rotations of the vehicle's axes. First with a pre-rotation (ϕ_{pre}) about the Z-axis, second by a tilt (θ_{tilt}) about the Y-axis and third by a post-rotation (ψ_{post}) again about the Z-axis. The pre-rotation (ϕ_{pre}), the tilt (θ_{tilt}) and the post-rotation (ψ_{post}) are defined as follows [23]:

$$\phi_{pre} = tan^{-1}\left(\frac{a_y}{a_x}\right), \tag{4.1}$$

$$\theta_{tilt} = cos^{-1}\left(a_z\right), \tag{4.2}$$

$$\psi_{post} = tan^{-1}\left(\frac{-a_x sin\left(\phi_{pre}\right) + a_y cos\left(\phi_{pre}\right)}{\left(a_x cos\left(\phi_{pre}\right) + a_y sin\left(\phi_{pre}\right)\right) cos\left(\theta_{tilt}\right) - a_z sin\left(\theta_{tilt}\right)}\right). \tag{4.3}$$

To determine the orientation of the accelerometer in the *Nericell* system the median

values of the accelerometer data (a_x, a_y, a_z) over a 10-second window are used to continuously compute estimates for the ϕ_{pre} and θ_{tilt} [23]. A change in the estimates of ϕ_{pre} and θ_{tilt} suggests a change in the orientation of the accelerometer. Very subtle rotations of the accelerometer about Z would be unnoticed according to Mohan et al [23]. Following a change in the continuously computed estimates of ϕ_{pre} and θ_{tilt} the estimate of ψ_{post} is continuously computed when deceleration is noticed from the GPS receiver data. The mean values of the accelerometer data (a_x, a_y, a_z) during the first few seconds of the deceleration period are recorded and used together with the estimates of ϕ_{pre} and θ_{tilt} to estimate ψ_{post}. The estimates of ϕ_{pre}, θ_{tilt} and ψ_{post} are used to estimate the compensated values (a'_X, a'_Y, a'_Z).

In P^3 the 3-axis accelerometer along with the GPS receiver data are collected in the *Collecting sensory data* layer (Fig. 4.1) [37]. The P^3 was implemented as an Android platform mobile application and a single workstation PC was used for the implementation of the data center clustering. Samsung Galaxy Nexus 3 and Google Nexus 4 smartphones with embedded accelerometers (200 Hz) were used to collected the data in different vehicles. The wheelbase information of the vehicle is acquired based on the type and brand of the vehicle that are defined by the user. The wheelbase information is required for perceiving the accurate pothole profile. In the *Pre-processing acceleration data* (Fig. 4.1) layer the background noise in the data (running engine, unsmooth road surface) are mitigated. Moving average mehtod is used to mitigate the background noise in the data. After the mitigation of the background noise the data is segmented using a sliding window. The consecutive segments with values exceeding the overall road variance times three are combined as the vibration signal for pothole detection.

For the developing the different algorithms proposed by Mednis et al external accelerometers were used to collect the data at 100 Hz and uploaded to a laptop computer [20]. For the evaluation of the developed algorithms four different smartphones at different accelerometer sampling rate (16, 98, 52 and 47 Hz respectively) were used. A test-track with the length of 4.4 km was driven for 10 laps to collect the data for evaluation. The test-track contained in total 108 different road anomalies which were marked as ground truth events.

4.1.2 Detection method computation

In the P^2 system the *pothole detector* detects potholes and other road anomalies from the raw 3-axis accelerometer data based on their reflections in the data [11]. The data is processed immediately after it is received from the accelerometer. Each received data trace is segmented into 254 sample windows and a continuous stream of windows

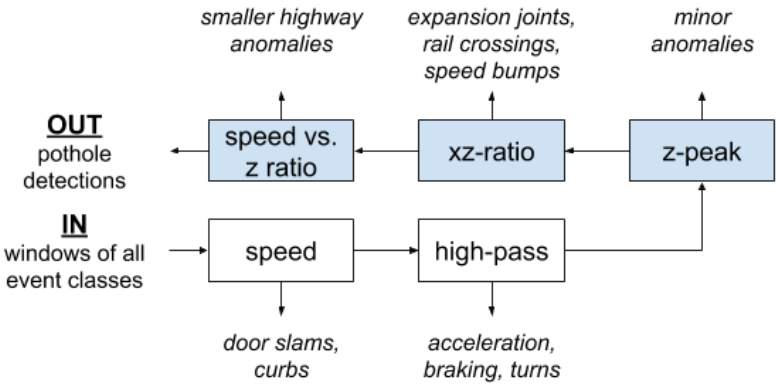

Figure 4.2: The pothole detector is composed of a number of filters in sequence, each separating out a different class of event [11].

from the received traces are processed with a series of signal processing filters. The *pothole detector* uses the series of filters to reject one or more normal events reflected in the data and finally to single out the detected potholes reflected in the data. Figure 4.2 illustrates the series of filters used in the *pothole detector* [11]. From the aligned accelerometer data the measurements from along the vehicle's lateral X-axis and vertical Z-axis are considered in the filters. The first filter (*speed filter*) rejects normal event reflections based on the speed of the vehicle. This filter rejects reflections in the accelerometer data which occur during in slowly moving or a stationary vehicle. The second filter (*high-pass filter*) rejects additional normal events like acceleration, braking, veering and sudden sensor orientation changes. Such events are reflected as low-frequency reflections on both x and z axes of the accelerometer data. The rest three of the filters each use a filter specific adjustable threshold parameter to filter out some of the reflections of normal events. Eriksson et al conclude that the road anomalies usually have significant reflection on the vertical z-axis of the accelerometer data [11]. Therefore the third filter (*z-peak filter*) rejects reflections in which the absolute values of the z-axis frequencies are less than the filter specific threshold t_z. Eriksson et al assume that potholes only impact on one side of the vehicle and generate a significant reflection in the horizontal x-axis within some time interval after a significant reflection on the vertical z-axis [11]. Based on this assumption the fourth filter (*xz-ratio filter*) rejects reflections in which the x-axis peak reflection is less than the filter specific threshold t_x times the peak reflection in z-axis, during the time interval. High-speed can create high peak reflections to the data from small road anomalies. The fifth filter (*speed vs. z-ratio filter*) rejects reflections where the z-axis peak is less than the filter specific threshold t_s times the speed of the vehicle. A simple machine learning approach of combined brute-force search over the interval of reasonable values is used to assign values for the set of threshold parameters $t = \{t_z, t_x, t_s\}$. The detec-

tor score, $s(t) = corr - incorr^2$, is computed for each threshold set t, where *corr* is the number of potholes in the manually collected training data set, and *incorr* is the number of other road anomalies in the training data set [11]. The latter is squared to minimize the false-positive detections. The detection algorithm in the *pothole detector* uses the threshold set t as a classifier which maximizes the score $s(t)$. The *loosely labelled* training data do not include locations and time of the encountered potholes but it contains rough estimates of the number of detections, $count_r$, to be expected on a road section. The detector score with the *loosely labelled* data embedded is as follows $s(t) = corr - incorr^2_{labelled} - max(0, incorr_{loose} - count_r)$ [11]. The number of detection errors on labelled data ($incorr_{labelled}$) is squared to emphasize the more reliable nature of the hand labelled training data against less reliable *loosely labelled* training data.

In the *Nericell* system Mohan et al used a similar simple machine learning approach as was used in the P^2 system by Eriksson et al [23]. The *Nericell* system was trained to detect bumps or potholes as a single type of road anomaly. The distinction between these two types road anomalies was assumed to be made in the post-processing from the detection data. When comparing to the P^2 system in the *Nericell* system slight change was made to the series of the signal processing filters. Mohan et al had made an observation that the magnitude of the acceleration measurements varies in the z-axis depending on the speed of the vehicle [23]. For this reason they used a different filter depending on the speed at which the accelerometer data was collected. The same *z-peak filter* from the P^2 system was used with speeds over 25 km/h and a different *z-sus* filter with lower speeds. The *z-sus* filter looks for sustained dips on the accelerometer z-axis that are under some threshold T for the period of at least 20 ms [23].

In the P^3 system potholes as the road anomalies are detected with a similar method as described in the P^2 system in the *Pre-processing acceleration data* layer (Fig. 4.1) [37]. In the *Perceiving pothole profile* layer with the *active vibration recovery* algorithm the inherent attributes of the vehicle are learned from the underdamping vibrations generated right after the wheel of the vehicle has hit a pothole. With the learned information the vibrations of the wheel can be recovered by adopting single degree-of-freedom vibration model (*One-DOF*) [37]. The *Active vibration recovery* algorithm in the P^3 system adopts the *One-DOF* model to perceive the profile of an individual pothole. In the adopted *One-DOF* model the vehicle chassis is connected to upper end of a suspension system of consisting a spring and a damper. The suspension system is connected from the lower other end to a wheel. According to Xue et al the relation between the vertical shift distance of the vehicle chassis and the wheel is

formalized as

$$c\ddot{y} + ky = m\ddot{x} + c\dot{x} + kx, \tag{4.4}$$

where m is the vehicle mass, k is the coefficient for the spring, c is the coefficient for the damper, x is the vertical shift of the vehicle body, $\dot{x}$ is the derivative of x, $\ddot{x}$ is the second derivative of x and y is the vertical shift of the wheel [37]. According to Xue et al the above relation (Eq. 4.4) can be solved and deduced as follows

$$\begin{cases} y = e^{-\frac{k}{c}t}\left[\int q(t)e^{\frac{k}{c}t}\mathrm{d}t + a\right] \\ q(t) = \frac{m}{c}\ddot{x} + \dot{x} + \frac{k}{c}x \end{cases}, \tag{4.5}$$

where a is a constant and is assigned as 0, $\ddot{x}$ is the z-axis readings from the accelerometer, $\dot{x}$ and x are integrals of $\ddot{x}$ and $\dot{x}$ along time, respectively [37]. The inherent attributes of the vehicle, $\frac{m}{c}$ and $\frac{k}{c}$, are required to derive y with $\ddot{x}$ [37]. The vibration process generated to the vehicle when driven over a pothole consists from a forcing vibration and a underdamping vibration according to Xue et al [37]. The forcing vibration starts when the wheel of the vehicle enters into the pothole and lasts until it leaves the pothole. The underdamping vibration starts when the wheel leaves the pothole and lasts until the vehicles natural vibration has gradually decreased to zero on an even road surface. With this the value of y is assigned to 0 and the relation (Eq. 4.4) is transformed as follows

$$\ddot{x} + \frac{c}{m}\dot{x} + \frac{k}{m}x = 0 \rightarrow \ddot{x} + 2n\dot{x} + p^2x = 0, \tag{4.6}$$

where $n = \frac{c}{2m}$ and $p = \sqrt{\frac{k}{m}}$ [37]. From the underdamping vibration with $n < p$, the result of the transformed relation in Eq. 4.6 is

$$x = Ae^{nt}sin\left(\sqrt{p^2 - n^2t} + \alpha\right), \tag{4.7}$$

where A is the initial amplitude and α is the phase of underdamping vibration [37]. From the result in Eq. 4.7 it can be seen that the underdamping vibration periodicity, T, is fixed as

$$T = \frac{2\pi}{\sqrt{p^2 - n^2}} \approx \frac{2\pi}{p} \rightarrow p = \frac{2\pi}{T}, \tag{4.8}$$

according to Xue et al [37]. The result is the frequency of the underdamping vibration p and it depends only on k and m. The effect of the damper is the amplitude attenuation rate of the underdamping vibrations, η, defined as

$$\eta = \frac{A_i}{A_{i+1}} = \frac{Ae^{-nt}}{Ae^{-n(t+T)}} = e^{nT} \rightarrow n = \frac{ln\,(\eta)}{T}, \tag{4.9}$$

where A_i and A_{i+1} are the amplitudes of two consecutive vibration waves, respectively [37]. With the Eq. 4.8 and Eq. 4.9 it is possible to estimate y during the forcing vibration as

$$y = e^{-\frac{p\pi}{\delta}t} \int q\,(t)\, e^{\frac{p\pi}{\delta}t} \mathrm{d}t, \tag{4.10}$$

where δ denotes $ln\,(\eta)$ [37]. After vibration recovery the depth and the length of the pothole are estimated and used as the profile of the pothole. The depth estimate is corrected with a linear model based on the distance and the width of the wheelbases of the vehicle. The length estimate is computed by multiplying the speed of the vehicle with the time the wheel was in the pothole. In the *Aggregating individual perceptions* layer (Fig. 4.1) the aggregation algorithm is used to get more accurate profile estimations from the different individual pothole perceptions [37]. The perceptions of the same pothole are clustered with *K-means* algorithm according to the depth attribute. The optimal number of clusters k is determined with a gap statistic method. A cluster with at least k number of perceptions and maximum average depth is chosen for aggregation. The perceptions are weighted based on the speed of the vehicle and sampling rate of the accelerometer. Perceptions with lower speed and higher sampling rate are assigned with a weight of more confidence. The accurate pothole profile is the aggregated result of the weighted average depth and width of the individual perceptions.

The approach in the system described by Mednis et al is similar as used in the P^2, the *Nericell* and the P^3 systems [20]. As with the *z-peak* and the *z-sus* algorithms in the P^2 and the *Nericell* systems the algorithms described by Mednis et al could be used similarly in conjunction with other algorithms (e.g. noise reduction filters) to detect road anomalies. The *Z-THRESH* detection algorithm is similar to the *z-peak* algorithm used in the P^2 and the *Nericell* systems. A pothole is detected based on the accelerometer z-axis values that exceed a specific thresholds reflecting the size of the pothole. The *Z-DIFF* is slightly more advanced algorithm which searches for two consecutive values from the accelerometer z-axis measurements with a difference that exceeds a given threshold. The algorithm detects all fast enough changes in the vertical z-axis. Both the *Z-THRESH* and the *Z-DIFF* algorithms assume a well-oriented alignment of the accelerometer's coordinate frame with the vehicle's coordinate frame. The *STDEV(Z)* algorithm uses a standard deviation of the measurements from the z-axis. In the algorithm a sliding window size and a threshold value need to be specified for pothole detection. The *G-ZERO* algorithm is based on the observation of events from the accelerometer measurements with near zero gravity values on all three axes. Mednis et al concluded that zero gravity events are created when the vehicle enters or leaves a pothole [20].

4.1.3 Performance evaluation of the methods

The P^2 was evaluated in four steps [11]. In step *Classification accuracy on hand-labelled data* the hand-labelled data was randomly split 100 times into test and training sets. The detector was trained with each training set and tested for accuracy with the corresponding test set. The average of the results was used as a baseline performance measure. In step *Performance improvement using loosely labelled training data* the *loosely labelled* data was used to fine-tune the trained detector to see the improvement in the accuracy of the detector. The result on false-positive detection rate of road anomalies improved after the fine-tuning of the detector. E.g. the actual pothole detection rate improved from 88.9 % to 92,4 % and the false-positive detection of expansion joints as potholes dropped from 2.7 % to 0.3 %. In step *Performance on loosely labelled roads* the fine-tuned detector output was compared with the expected results from the roads used to collect the *loosely labelled* data. The results from this step showed false-positive detection rate on smooth roads was 0.15 %. In step *Spot-checks on uncontrolled data* the 48 highest-confidence detections were manually verified on the detection spot. The uncontrolled data included normal events reflected from normal usage, such as door slams and unusual driving behaviour. With such data and the cluster-based filter size of four, 48 detections were made with 39 of them were potholes which required attention. Three data sets were used in the evaluation: hand-labelled data, loosely labelled data and 10 days worth (9 730 km) of recorded data with the *pothole detector* deployments in the taxis. The false-positive detections are usually single detections at some location at some point in time [11]. Such false-positive detections are filtered with a cluster-based filter in the P^2 central computing unit to improve the real detection accuracy. A cluster is formed when at least k number of detections within the distance of Δt occur in the same location, with a marginal error of Δd. The centroid of the locations of the detections in the cluster is reported as a location of a cluster denoting a pothole. Pothole-like road anomalies which do not actually require attention can also produce false-positive detections according to Eriksson et al [11]. Blacklisting of such detections in the P^2 central computing was used to remove them from the final results.

Mohan et al evaluated the *virtual reorientation* algorithm used in the *Nericell* system by collecting measurements of acceleration and braking (X-axis) events during driving [23]. Measurements were taken with two well-oriented accelerometers and with one disoriented accelerometer. With the measurements from the disoriented accelerometer pre-rotation, tilt and post-rotation were estimated and used together with values a_x, a_y and a_z to estimate the values a'_X, a'_Y and a'_Z as the estimated orientation of the vehicle. To assess the accuracy of the *virtual reorientation* algorithm a cross-correlation

value r between the time-series of the estimated values (a'_X, a'_Y, a'_Z) and the measured values a_X, a_Y and a_Z from the well-oriented accelerometers were computed. Due to the noise in the data only the periods of interest, like braking or a bump, were considered in the cross-correlation. During such periods the cross-correlation was computed between all three accelerometers. In general the cross-correlation result significantly improved when comparing the results of disoriented measurements to the results of measurements compensated by the *virtual reorientation*. The cross-correlation results after the *virtual reorientation* were aligned with the cross-correlation results between the two well-oriented accelerometers. The cross-correlation results were high but still significantly less than perfect ($r = 1$) due to noise which was mitigated by focusing on the more sustained surges (braking) instead of to momentary spikes according to Mohan et al [23]. The results suggested that for road anomaly detection the measurements from the disoriented accelerometer with the *virtual reorientation* were almost as accurate than with the well-oriented accelerometer. The braking detection in the *Nericell* system was evaluated against the ground truth speed which was established based from a series GPS location estimates. The ground truth braking was observed when the deceleration of at least 1 m/s was detected over at least 4 seconds. The same heuristics were used to detect braking event from the acceleration measurements. The ground truth and the acceleration measurements were collected from the same drive with one well-oriented and one disoriented accelerometer. The disoriented accelerometer measurements were compensated with the *virtual reorientation* algorithm. The comparison of the results indicate that the *virtual reorientation* of disoriented accelerometer maintains the characteristics of the measurements adequately for the braking detector to work properly. False-positive rates were high (15-31 %) which were still considered to be caused by the lesser magnitude deceleration events. False negative rate was low (4-11 %) again caused by borderline deceleration events according to Mohan et al [23]. Both false-positive and false-negative rates were interpreted to be affected by GPS localization error. The bump detector in the *Nericell* system was tested on two different road sections. Shorter road section of 5 km was labelled as *bumpy road* with 44 road anomalies and a longer road section of 30 km was labelled as *mixed road* with 101 road anomalies. The acceleration measurements were obtained with one well-oriented accelerometer and with one disoriented accelerometer with the *virtual reorientation* compensation. The detection results showed high false-positive rate (20-30 %), which was partly interpreted to be caused by the difficulty in manual labelling according to Mohan et al [23]. Also with the bump detection results the false positive/negative rates indicate that the *virtual reorientation* maintains the characteristics of the measurements of the disoriented accelerometer.

For the evaluation of the P^3 system a trace of 2 760 segments of accelerometer

data was collected from roads in urban areas [37]. 23 different potholes were manually profiled as the ground truth. Different vehicle speeds with different accelerometer sampling rates, smartphone placements and different sides of the vehicle impacted by a pothole (side-wheel) were considered as the data was collected. The error rate metric (ε),

$$\varepsilon = \left[\frac{d_{estimate} - d_{real}}{d_{real}} \right], \tag{4.11}$$

was used in the performance evaluation where $d_{estimate}$ is the estimated pothole length or depth and d_{real} is the ground truth pothole length or depth respectively [37]. For the evaluation of the speed and sampling rates Xue et al reported that in general a good suspension system of the vehicle and a higher sampling frequency of the accelerometer improves the pothole profile estimation accuracy in higher speeds. In low speeds the P^3 system is able to achieve good estimation results. For the depth estimation using 200 Hz sampling frequency 9 % error rate was achieved in 10 km/h and 12 % error rate in 20 km/h. For the length estimation the error rate was reported to be slightly larger. With smartphone placement in the vehicle Xue et al reported that the error rate was more stable and accurate when the smartphone was placed in the center of the vehicle. Also with the different side-wheel impacts the error rate increased when the smartphone was not placed in the center of the vehicle. In overall the performance evaluation results varied a lot and the cases where better suspension system with higher sampling rate was used the P^3 system was able to estimate at best 90 % of the pothole depths with 10 % error rate, and 90 % of the lengths with 20 % error rate. The results were achieved by using a linear error correction model which decreased the estimation error rate by 2-3 % units.

The performance of the four algorithms introduced by Mednis et al was evaluated with the following steps [20]. First, the ground truth potholes were marked on the selected test track. The accelerometer measurement data was collected by driving the test track. Collected data was processed using the different detection algorithms. Statistical analysis was performed of the algorithm's performance on current and historical knowledge of the ground truth. The historical knowledge ground truth was obtained from another study conducted earlier by Mednis et al [20]. Both current and historical ground truth contained 5 classes of potholes: large potholes, small potholes, pothole clusters, gaps and drain pits. The performance evaluation results of the different algorithms are presented in Table 4.1. For clarification, the different types of road anomalies and respectively the number and percentage of detected as a road anomaly are presented for each of the road anomaly. It appears that the algorithms are capable to detect a road anomaly with any of the types but the algorithms are still incapable of detecting the type of the road anomaly.

Table 4.1: True positive rate of four algorithms [20].

Class	Z-THRESH	Z-DIFF	STDEV(Z)	G-ZERO
Large potholes	3 (100 %)	3 (100 %)	3 (100 %)	3 (100 %)
Small potholes	15 (83 %)	16 (89 %)	16 (89 %)	14 (78 %)
Pothole clusters	25 (83 %)	27 (90 %)	27 (90 %)	27 (90 %)
Gaps	31 (78 %)	36 (90 %)	30 (75 %)	27 (68 %)
Drain pits	10 (59 %)	17 (100 %)	11 (65 %)	8 (47 %)
Total	**84 (78 %)**	**99 (92 %)**	**87 (81 %)**	**79 (73 %)**

4.2 Classification of road anomalies

In this section different approaches of Support Vector Machine (SVM) classifier for classifying the road anomalies are discussed through the methods introduced in [8, 25, 5]. SVM classifier can be trained to classify data to multiple different classes. To train a multi-class SVM classifier a labelled training data set is required. Exception of SVM is the one-class SVM classifier which is trained with a training set containing unlabelled data of one class. As the training data in the case of one-class SVM classifier is unlabelled the method is considered as an unsupervised learning method by some. It is also be considered as a semi-supervised learning method when large amount of unlabelled training data of one class with considerably less anomalous data is used to improve the classification accuracy. One-class SVM classifier is considered as an anomaly detection method as it is trained to detect new data samples which differ from the data samples it was trained with as anomalies.

In a study by Hautakangas, Nieminen, Mazhelis, Perttunen, Riekki, Ristaniemi, Gou, Hou and Zeng wavelet packet decomposition (WPD) and one-class support vector machine (SVM) classification algorithm were used as a approach to detect potholes from 3-axis accelerometer measurements [8]. The pothole detection approach contains the feature extraction, feature selection and classification phases. The acceleration measurement data, especially in the case when the wheel of the vehicle hits a road anomaly (e.g. pothole), is collected with an accelerometer attached to a moving vehicle. As the signal from the road anomalies reflected in the accelerometer measurements is affected by the vehicle movement the collected data is required to be transformed in the feature extraction phase. WPD was used for the feature extraction as Hautakangas et al had recognized the feasibility of the wavelet transformation for road anomaly detection [8]. To train the pothole detection classifier four different feature selection methods were evaluated to select the best performing feature selection method. The classifier was trained to classify the samples into two different classes with a semi-supervised

one-class SVM classification method as the number of road anomaly sections in the acquired data was much smaller than the normal road sections. In the one-class SVM classification method the classifier was trained with data from normal road sections and tested with separate data from normal and anomalous road sections.

Seraj, van der Zwaag, Dilo, Luarasi, Havinga, Atzmueller, Chin, Janssen, Schweizer, and Trattner investigated wavelet decomposition analysis and Support Vector Machine (SVM) classifier to build a real time road anomaly detection and classification system the *RoADS* for Android platform smartphones with embedded inertial sensors and GPS receiver in [25]. The vehicle vibrations caused by the different road anomalies when driven over a such were measured both with the accelerometer and the gyroscope sensors. The idea with the *RoADS* system was to detect different types or classes of road anomalies (not only potholes) with the same detector. Figure 4.3 illustrates an overview of the *RoADS* system as a flow chart.

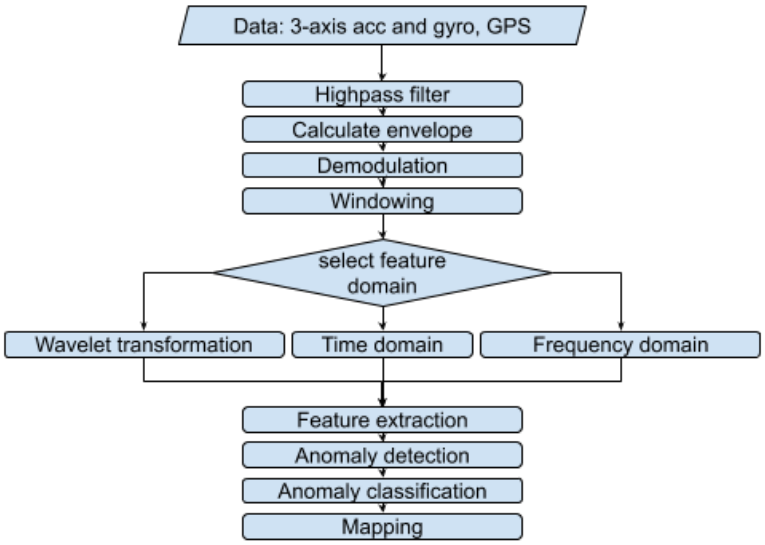

Figure 4.3: RoADS system overviews as flow chart [25].

Aragón, Carlos, González and Escalante proposed a *Pattern Recognition Pipeline* to sense the road conditions by identifying and classifying the road anomalies based on the accelerometer measurements from a smartphone [5]. In this approach Support Vector Machine (SVM) classifier is used to segment the accelerometer measurements by classifying them into non-anomalous and anomalous classes and then use Random Forest algorithm to classify the different anomalies. The approach taken with the SVM classier by Arag'on et al is introduced in more detail in their later work [6].

4.2.1 Collecting and preprocessing the raw data

In the *data collecting* phase for the one-class SVM classification method the data was collected using a vehicle mounted Nokia N95 smartphone which contained a 3-axis accelerometer (38 Hz) and a GPS receiver [8]. The accelerometer coordinate frame was aligned with the vehicle where X denoted the longitudinal axis and pointed to the front of the vehicle, Z denoted the lateral axis and pointed to the right and Y denoted the vertical axis and pointed to up. The naming of the triad axes differs in this approach from the one described in Section 3.1.2. Three different cars were used to collect the data. Only the data from the vertical y-axis as was used to detect potholes as Hautakangas et al had found that the other axes did not contain any significant changes when driven over a pothole [8]. The data was labelled to consist 21 segments with potholes and 1764 segments with normal road. Each segment was 3 seconds long and a Hamming window function was used to symmetrise the data in a segment around the maximum in the middle to avoid losing any high energy spikes from the data. In *feature extraction* phase WPD low-pass and high-pass filters were used to recursively decompose the signal into approximation and detail coefficients of variance at the end nodes of the resulting tree structure. The coefficients of variance were regarded as the signal's features. The *Daubechies wavelets* wavelet family was selected for the decomposition since it has been commonly used in the wavelet based analysis and its frequency responses with the selected parameters match the spectral properties the accelerations caused from a pothole. The number of levels to decompose the signal was set to 7 since $7^2 = 128$ was approximately the number of samples in a segment 3 s $\times$ 38 Hz = 114. 128 features were extracted from the samples in a segment. Based on analysis of the power spectrum of the potholes and the normal road segments the WPD features from the frequency interval of 1.5 Hz to 10 Hz were selected. Finally 30 WPD features (#5 - #34) were chosen for the *feature selection* phase after normalizing the features with standard deviation. For the feature selection a feature selection method was used to find the best features discriminating the potholes and normal road segments. Four commonly used methods for selecting the best features were tested and evaluated: Forward Selection (FS), backward selection (BS), genetic algorithm (GA) and principal component analysis (PCA). FS is a stepwise selection method to select a subset of features which give the best result compared to other subset of features. FS starts with no selected features. First the feature with the best classification result (e.g. statistical f-test) is selected. Next the feature from the unselected features which in combination with the already selected feature give the best result gets selected. The procedure continues by comparing an unselected feature together with the selected features until there are no more unselected features left that

would increase the result or increases the result only a little or a predefined upper limit for selected features is reached. BS is similarly a stepwise selection method like FS but works in opposite direction. Initially classification is performed with all features. The procedure continues by selecting the feature which decreases the classification result the most until the result does not decrease or decreases only a little or a predefined upper limit of features are removed. GA is a computational model that searches potential solutions to a problem e.g. selecting a subset of features for SVM. The algorithm starts with randomly selected initial population from the original data set. The individuals in the population are described with a binary vector of length m as the number of features. The binary vector is called a chromosome and the bits represent whether the feature (a gene) for that individual is present (1) or not (0). The algorithm selects the best individuals depending on a fitness score given by a fitness function based on the individual's fitness to the problem. Next the algorithm performs crossover for the pairs of selected individuals to produce new offspring to the population. In crossover the produced offspring will inherit some of its genes from either of the parents. After the crossover the algorithm randomly decides, with a low probability, whether the offspring is subject to mutation or not. In mutation some of the genes of the offspring are flipped to prevent premature convergence. The procedure of selection, crossover and mutation is repeated until there is no significantly better offspring being produced. PCA is used to find uncorrelated principal components which explain the dependencies between the features. Most of the variance in the data is usually explained by the first principal component. PCA is produced by performing eigenvalue decomposition of the covariance matrix of the extracted feature dataset. All the feature selection methods were used to train one-class SVM and their performance was evaluated. Based on the evaluation results Hautakangas et al concluded that PCA was clearly the best feature selection method when the number of selected features is greater than 5 and FS was the best with the number of selected features from 2 - 6 [8].

The *RoADS* system was used to detect and classify road anomalies on a road with asphalt or concrete surface layer [25]. All disruptions from the smooth surface were considered as road anomalies. With too few individual road anomalies for classification the road anomalies were divided and labelled into three classes: *Severe*, *Mild* and *Span*. *Severe* class contained sunk-in manholes, small potholes and deteriorated or heavily patched road surface segments. *Mild* class contained anomalies affecting only one side of the vehicle, such as one side patches or bumps. *Span* class contained road-wide anomalies, such as bumps, road extension joins, patches and thick paint. Five different types of vehicles were used to collect the data from different roads in two different cities in different countries (Albania, Netherlands). Data from total of 100.3 km and 45.9 km of unique roads were collected over 5 trips. Windscreen attached Samsung

Galaxy S2 smartphones with Android 4.0 and Inertia ProMove 3D software were used to measure the vehicle vibrations. Approximately $\frac{3}{4}$ of the total roads were measured at 47 Hz and $\frac{1}{4}$ at 93 Hz accelerometer frequency. The smartphone orientation used in the *RoADS* system was with an aligned coordinate frame orientation with the coordinate frame of the vehicle, where Z-axis is longitudinal and points to front, Y-axis lateral and points to left and X-axis is vertical and points to up. Also in this approach the naming of the triad axes differs from the one described in Section 3.1.2. Similarly as with the assumptions made in Section 3.2 also Seraj et al had concluded that when the vehicle experiences a road anomaly the effect can be measured both from the vertical acceleration of the vehicle and from the angular velocities of the rotational movements of the vehicle [25]. An assumption that the accelerometer placed in the vehicle measures only the effect of gravity when travelling a smooth road with constant speed was used. When a pothole is experienced with one-side of the vehicle the lateral Y and the vertical X displacement of the vehicle is measured by the accelerometer y and x axes. Likewise the orientation of the vehicle is changed by the experience with a roll angle of the Z-axis and the changed angular velocity is measured by the gyroscope. On the other hand when a road-wide anomaly, like a speed bump, is experienced then only the vertical x-axis of the accelerometer is measuring the change and the orientation change is measured by a pitch angle of the y-axis with the gyroscope. Seraj et al had noticed that the vehicles were equipped with a suspension system which attenuate vibrations of the vehicle from road anomalies [25]. Similarly they had noticed that the speed of the vehicle effects the vibrations of the vehicle when experiencing a road anomaly. The phenomenon was called *speed dependency*. It is important to consider the speed of the vehicle to compensate the effect of speed in the accelerometer measurements as the envelope (a smooth curve outlining the extremes of the oscillating signal) of the accelerometer measurement absolute values follows the GPS speed signal. The complex mechanical vibrations in a signal measured by the accelerometer is modulated from different signals. In this respect the accelerometer signal is like a carrier signal containing other signals like the speed, slope degree, engine and tyre revolutions. According to Seraj et al in *Hilbert-Huang transform* the empirical mode decomposition (EMD) of complex mechanical vibrations is done with *envelope demodulation* [25]. The demodulated signal dS of raw signal S is obtained with

$$dS\left(t\right) = \frac{H \circ S\left(t\right)}{E \circ \left|H\right| \circ X_{acc}\left(t\right)}, \tag{4.12}$$

where t is time, $\circ$ is the function composition, E is the moving average filter, H is high-pass filter applied to the signal and X_{acc} is the x-axis accelerometer measurements [25].

The moving average filter E is

$$E\left(t_i\right) = \frac{1}{M} \sum_{j=0}^{M-1} X\left(t_{i+j}\right), \tag{4.13}$$

where M is a 2000 samples rolling window [25]. After the speed, slope and the other low-frequency components are mitigated the road anomaly amplitudes in the signal are more uniform but still the amplitudes varies depending on the characteristics of the vehicle when driven over a road anomaly. The different vibrations happen at a certain frequency band. These vibrations include for example the engine revolutions and wheel revolutions. The vibration frequency caused by a road anomaly depends on the wheel and tyre characteristics as well as from the road anomaly characteristics. When the vehicle is standing still in e.g. traffic lights or moving very slowly in traffic jam the vibrations are minimal and the variance of the low-frequency vibration signal is close to zero. The low-frequency vibration segments of the signal were discarded with the highpass filter (first order butterworth highpass filter). For classification the features from the accelerometer and the gyroscope measurement data were extracted by computing from the time domain, by transformation into frequency domain and by wavelet decomposition. For the extraction the data was windowed to 2.5 s samples which corresponds to 256 samples with 170 samples overlapping for 93 Hz data, and 128 samples with 85 samples overlapping for 47 Hz data. The features extracted from the time-domain were mean, standard deviation, variance, peak-to-peak, root mean square, zero crossing rate, mean of absolute value, correlation between all axis, tilt angles, wave form length and signal magnitude area. After Fast Fourier Transform with Hamming window the features extracted from frequency-domain were mean frequency, median frequency and energy of the frequency bands. According to Seraj et al the wavelet decomposition was done with Stationary Wavelet Transfrom (SWT) and defined as Sym5 wavelet from the symlet wavelet family after experimenting with different wavelet families [25]. Four levels of wavelet decomposition was giving the appropriate result. The features extracted from SWT decomposition were absolute mean, standard deviation, variance and every energy level of both detail and approximation.

A number of road anomaly samples were collected with an Android platform smartphone device with an embedded accelerometer at 50 Hz sampling frequency [5, 6]. The device's coordinate frame of reference was aligned with the vehicle's coordinate frame of reference in the same manner as described earlier in this thesis in Section 3.1.2. Total of 237 samples of road anomalies such as speed bumps, potholes, metal bumps and plane road were collected and stored into an external database. The database was used to create the training and test datasets with both total of 30 homogenous and heterogeneous virtual roads with different number of different road anomalies in each. Based on the chosen number of each road anomaly type virtual road datasets

containing concatenated acceleration samples of non-anomalous and anomalous roads were created from the database. To segment the samples of all virtual roads into non-anomalous and anomalous road segments a sliding window method was used [5, 6]. Twelve features were selected in a manner that no useless or redundant feature was in the selection. The selected features were 5 statistical features and 7 other features to enrich the statistical information. The statistical features selected were the mean of the accelerometer values, standard deviation, variance, coefficient of variation and the difference between maximum and minimum accelerometer value. Four of the other features used to enrich feature vector were a confidence scores of 4 of the earlier mentioned statistical features (not including variance). The confidence scores was determined by comparing each of the values of the 4 statistical features to a corresponding threshold values. If the statistical feature value was over the corresponding threshold value the respective confidence score was 0.8 and 0.2 otherwise. The number of times a statistical feature overpassed a threshold was selected as another feature. As the last two features the sum of confidence values and its confidence value were selected. The features of the previously mentioned feature vector is illustrated in Table 4.2. For the classifier in the first classification stage Artificial Neural Network (ANN), Decision Tree (DT), Gradient Boosting Classifier (GB), Hidden Markov Model (HMM), Naive Bayes (NB), Nearest Centroid (NC) and Random Forest (RF) machine learning algorithms were evaluated together with the SVM. The segments classified as anomalous road in the first phase are further classified based on the type of anomaly in the second classification stage [5].

Table 4.2: The features and thresholds used to for the feature vector for SVM classification [6].

#	**Type**	**Feature**	**Threshold**
1	statistical	Mean	
2	statistical	Standard deviation	
3	statistical	Variance	
4	statistical	Coefficient of variation	
5	statistical	Difference Max-Min	
6	confidence	*Mean*	$g \times 0.3$ [1]
7	confidence	*Standard deviation*	$g \times 0.15$ [1]
8	confidence	*Coefficient of variation*	$g \times 0.015$ [1]
9	confidence	*Difference Max-Min*	$g \times 0.2$ [1]
10	statistical	Threshold overpasses	
11	statistical	Sum of confidence	
12	confidence	*Sum of confidence*	3

[1] g stands for gravity

4.2.2 Detection method computation

According to Hautakangas et al SVM classifier is commonly used to classify two classes but it can be extended to one-class or multi-class classification [8]. The one-class SVM classifier maps the input data to a higher dimension feature space and fits most of the data into a minimized hypersphere. All data points that fall outside of the hypersphere are considered as anomalies. One-class SVM classifier from the LIBSVM software package [7] was used with Gaussian radial base function (RBF) as the kernel and the hyperparameters (expected proportion of outliers) $\nu = 0.01$ and (decision boundary smoothness) $\gamma = 0.0002$. SVM classifier was trained with 1 234 segments of randomly selected normal road data. 530 segments of normal road data with 21 segments of road anomaly data was used to test the SVM model.

In the *RoADS* system a 2-step classification approach was utilized as it was assumed that the number of anomalous road windows is lower than the number of normal road windows [25]. In the first step, the anomaly detection, the anomalous road windows are classified apart from the normal road windows. In the second step, the anomaly classification, the detected anomalous road windows are classified by the type of the road anomaly. To train the SVM classifier 3 066 windows of labelled data was used with 2 073 window of normal roads and 993 windows of anomalous roads. Sliding window with 66 % overlap was used which resulted in some of the road anomalies to be present in several windows. 10-fold cross-validation was used in training the classifier with $\frac{1}{10}$ of both normal and anomalous roads used for testing in each iteration. Only the windows with the signal from a road anomaly spreading equally from the center of the window were used to train the detector as the anomalous road windows contained several windows with parts of the same anomaly due to the sliding window method. The best values for the hyperparameters used for the training were found with a grid search. For the anomaly detection kernel parameter (decision boundary smoothness) $\gamma = 0.002$ and (cost of misclassification soft margin constants) $C = 320$ were used. And respectively for the anomaly classification kernel parameter (decision boundary smoothness) $\gamma = 0.0002$ and (the cost of misclassification soft margin constant) $C = 100$ were used.

In the *Pattern Recognition Pipeline* each window was classified in the first step with a SVM classifier based on the 12 extracted features (Tab. 4.2) either to non-anomalous or anomalous road [5, 6]. Through experimenting with different setups Aragón et al found that a SVM classifier with *radial basis function* (RBF) kernel and the misclassification soft margin constant $C = 10$ resulted with the best performance. The types of anomalous road were normal road, pothole, asphalt bump and metal bump. For the second stage classifier (called the *Bag-of-Words* by Aragón et al) first

the training set was split with sliding windows to vectors, each with a descriptive class label. K-means algorithm was used to cluster the training samples (windows). The centers of the clusters were taken as *codewords* and a *codebook* was created from all of the *codewords* extracted from all of the training samples. The test data segmented in the first stage was further segmented into smaller sections with sliding window. The new smaller sections were compared to the *codewords* with Euclidean distance and the raw data segments were converted to histograms of *codewords*. After all segments had been converted the TF-IDF (term-frequency inverse document frequency) was applied to each window and attached to the conversion result, which was the feature vector to be classified with Random Forest classifier.

4.2.3 Performance evaluation of the methods

For the performance evaluation of the one-class SVM classifier Hautakangas et al used the average of 1000 SVM classifications [8]. When all 30 of the extracted features were used in the training and in the classification, the true-positives (TP) was 21, true-negatives (TN) was 524 and false-positives (FP) was 6. With this 100 % of the anomalies were detected and only in 6 cases a normal road section was mistaken as a road anomaly.

With the *RoADS* system Seraj et al experimented with different settings and combinations of the feature sets [25]. The best results for the anomaly classification were achieved with a combination of the features from the time domain and from the wavelet transformation (TD+SWT). For the anomaly detection only the SWT features were used for the classifier. The results from the different experiments conducted are presented in Table 4.3. The results of the experiments show that training the detectors with demodulated features result in more accurate classifiers than training with raw data. A anomaly classifier with wavelet decomposition features (SWT) and a classifier with combined features from time domain and wavelet decomposition (TD+SWT) were trained using 10-fold cross-validation. The results for the anomaly classifiers are

Table 4.3: Confusion matrix and accuracy for the classification of anomalous (positive) and normal (negative) segments of roads, with different feature sets [25].

Method	Accuracy	TP	TN	FP	FN	Spec.	Sens.	Prec.	G	RS	FPR	FNR
TD_{raw}	81.43 %	49	201	39	18	0.82	0.73	0.196	0.77	0.89	0.18	0.26
$\text{TD}_{demodulated}$	85.26 %	52	214	31	15	0.87	0.82	0.1955	0.84	0.94	0.13	0.18
FD_{raw}	77.88 %	49	194	51	18	0.79	0.73	0.2016	0.76	0.92	0.21	0.27
$\text{FD}_{demodulated}$	79.17 %	40	207	38	27	0.84	0.59	0.1619	0.71	0.70	0.15	0.40
SWT_{raw}	82.69 %	50	208	37	17	0.85	0.75	0.1938	0.80	0.88	0.15	0.25
$\text{SWT}_{demodulated}$	88.14 %	57	218	27	10	0.89	0.85	0.2073	0.87	0.96	0.11	0.15
$\text{TD+FD}_{demodulated}$	83.01 %	48	211	34	19	0.86	0.72	0.1853	0.79	0.83	0.14	0.28
$\text{TD+SWT}_{demodulated}$	88.78 %	59	218	27	8	0.89	0.88	0.213	0.89	0.99	0.11	0.12

TD = Time Domain, FD = Frequency Domain, SWT = Stationary Wavelet Transform
TP/FP = True/False positive, TN/FN = True/False negative, Spec./Sens. = Specificity/Sensitivity, Prec. = Precision
G = G-mean, RS = Relative sensitivity, FPR/FNR = False positive/negative rate

Table 4.4: Confusion matrix and accuracy of the classification of anomalous segments of roads, with features from SWT and TD+SWT [25].

	SWT			TD+SWT		
Class	Severe	Mild	Span	Severe	Mild	Span
Mild	17	3	0	16	4	0
Severe	1	15	0	0	16	0
Mild	0	0	9	0	0	9
Accuracy	91.1 %			91.1 %		

presented in Table 4.4. With both classifiers the overall accuracy is the same 91 % but the *Severe* class is detected slightly better by SWT with labelled data. Seraj et al also experimented with other feature sets but results were remarkably lower with accuracy less than 86 % [25]. Evaluation with unlabelled data was done with additional 5 trips to collect data from roads in the same two countries as for the training data. The results for the evaluation are presented in Table 4.5. The data was collected with the help of a labelling method to verify the results. Trips 1 and 2 were done using the same roads in Netherlands as with collecting the training data. Trips 3, 4 and 5 were done in Albania. For Trip 4 the video was corrupted resulting in incomplete evaluation. The results show that fewer anomalies detected in the Netherlands than in Albania because the drivers in Albania tried to avoid driving into road anomalies according to Seraj et al [25]. They also believe that some anomalies in Albania were not detected because the system was not trained for the type of the missed anomalies. The detectors performance of the *Severe* class was estimated by calculating the false-negative windows and the undetected anomalies from the recorded videos. The number of detections by the detector is greater than the number of mapped anomalies since the detector detects all windows with the anomaly, also the consecutive windows with the same anomaly. False detections (FP) are the number of severe anomalies detected

Table 4.5: The classification results for models with features from Time Domain and Wavelet Decomposition [25].

				Detection	Classification			Mapping	Evaluation			
		S/R	**#Win**	**Anom**	**Sev.**	**Mild**	**Span**	**mapped**	**Sev**	**TP**	**FP**	**MA**
Trip 1	TD	47 Hz	609	195	107	68	20					
	SWT	47 Hz	609	165	119	26	20	113	73	64	15	4
Trip 2	TD	93 Hz	764	222	76	105	41					
	SWT	93 Hz	764	207	93	72	42	123	61	52	12	3
Trip 3	TD	47 Hz	1067	280	119	106	55					
	SWT	47 Hz	1067	222	120	51	51	152	82	74	10	8
Trip 4	TD	47 Hz	2240	584	349	176	61					
	SWT	47 Hz	2240	412	255	98	59	296	173		no video	
Trip 5	TD	47 Hz	794	239	113	126	0					
	SWT	47 Hz	794	192	99	93	0	134	76	74	6	6

Sev. = Severe, TP = True detections, FP = False detections, MA = Missed Anomalies
mapped = number of anomaly points pinpointed on the map

as *Mild* anomalies. Missed anomalies (MA) are the number anomalies counted from the videos and not detected by the detector. Seraj et al conclude that regardless of the vehicle type and road location the system showed consistent accuracy of $\sim$ 90 % accuracy on detecting *Severe* road anomalies [25].

In the *Pattern Recognition Pipeline* the accuracy and F-measure performance evaluation results of the different algorithms experimented as the classifier for the first stage are presented in Table 4.6 [5, 6]. In terms of accuracy the results are very close to each other and with F-measure there are more differences. With both measure the SVM classifier is slightly performing the best with this dataset. The accuracy of the second stage classifier was done in two different ways. In the first one a candidate anomaly was extracted by an expert and RF was applied over the anomaly segments. The classification resulted with 83 % accuracy. In the second one the proposed pipeline with SVM was applied. The pipeline classification resulted with 71 % accuracy. When the SVM classifier was changed to one-class SVM classifier the pipeline classification resulted with 74 %. According to Aragón et al the total error of the proposed pipeline was 0.6584 [5].

Table 4.6: First stage classifier accuracy and F-measure results [5, 6].

	SVM	**ANN**	**DT**	**HMM**	**NB**	**NC**	**RF**
Accuracy	0.8151	0.8051	0.7337	*na	*na	0.7939	0.8033
F-measure	0.785	0.774	0.408	0.678	0.587	0.587	0.736

* na = accuracy results not available for HHM and NB in [5].

4.3 Detecting road surface roughness

In this section different methods for detecting the road surface roughness are discussed. The detection methods discussed here include a method with *C4.5 Decision Tree* for classifying anomalous and non-anomalous road sections, a method that utilizes *Linear Predictive Coding* to obtain an estimate of road surface roughness index for each sample of the road, and finally a regression method which utilizes a relationship found between a road roughness survey ratings and demodulated road surface signal.

Allouch, Koubâa, Abbes and Ammar proposed a real-time detection system for Android platform smartphones called the *RoadSense* to classify the road quality into two classes, namely to *Smooth* road and *Potholed* road classes [4]. The proposed system uses measurements from the smartphone's inertial sensors (accelerometer and gyroscope) to accurately predict the road quality. Three machine learning algorithms were evaluated as the classifier to be used in the system: *C4.5 Decision Tree* classifier,

two-class SVM classifier and *Naive Bayes* probabilistic classifier. The *C4.5 Decision Tree* algorithm builds a binary decision tree from the labelled training data set as the classification model. The *SVM* algorithm finds the hyperplane separating the two classes, based on labelled training data set, to be used in the classifier. The *Naive Bayes* algorithm builds a classifier that is based on the frequencies and combinations of the values in the labelled training data set. The *RoadSense* system is divided into training and prediction phases which are illustrated in Figure 4.4.

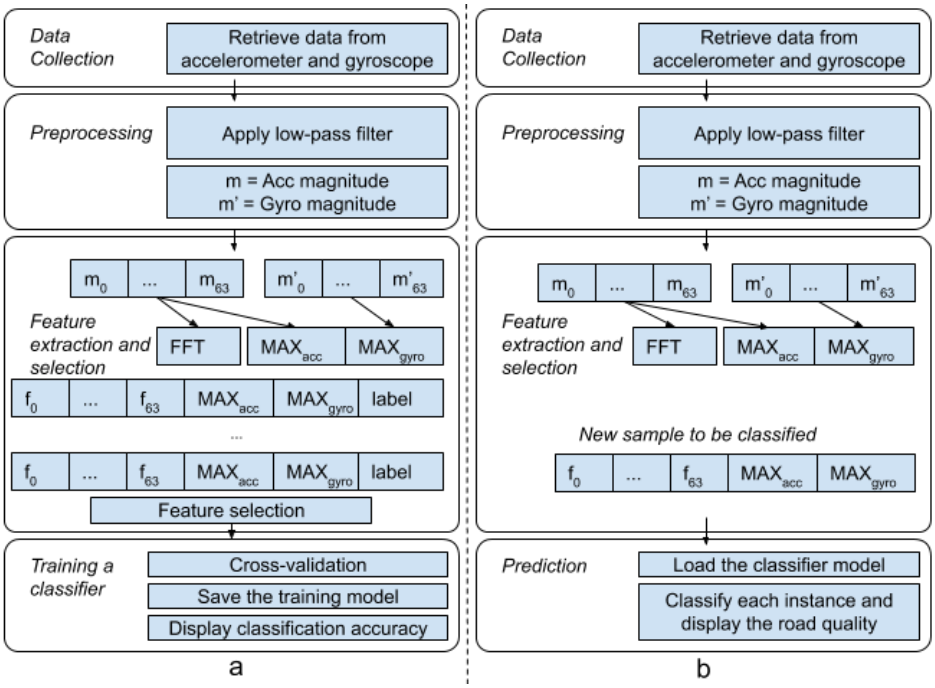

Figure 4.4: *RoadSense* flows: a) Training phase b) Prediction phase [4].

Alessandroni, Klopfenstein, Delpriori, Dromedari, Luchetti, Paolini, Seraghiti, Lattanzi, Freschi, Carini and Bogliolo proposed a system called *SmartRoadSense* for collaborative monitoring of road surface roughness in [3]. The system consists of a mobile application for Android platform smartphones to collect and process the accelerometer measurements and location data, a backend server to collect and aggregate the collected data from the smartphones and a graphical user interface for visualization of the collected data. *Linear Predictive Coding* is used in the mobile application to derive an estimate to obtain road surface roughness index from the accelerometer measurements. Instead of detecting the different spurious events (like potholes) from the accelerometer data the focus in the *SmartRoadSense* system is continuously monitoring the accelerometer measurements and assigning a numerical value to each sample of the road surface data to represent a roughness index of the road.

Aleadelat, Wright and Ksaibati proposed a method that uses the measurement data from the smartphone sensors together with data from road user survey to evaluate

the gravel road conditions [2]. To reduce the noise from the measurements caused by several sources a signal demodulation and a wavelet transformation was used on the sensor measurements. Aleadelat et al developed a regression model ($R^2 = 0.78$) to predict the overall *Riding Quality Rating Guide* (RQRG) rating for the travelled gravel road. The RQRG rating reflects the road users' perception regrading the quality of the gravel road. RQRG is a survey system based on visual assessment developed by Wyoming Technology Transfer Center. In the survey the gravel roads are rated on scale from 1 (failed) to 10 (excellent) and it is the most used rating system for gravel roads in the U.S [2].

4.3.1 Collecting and preprocessing the raw data

For the training phase of the *RoadSense* the measurement data from the embedded accelerometer and gyroscope sensors of a smartphone were collected [4]. The smartphone was mounted to the dashboard of the vehicle and the orientation of the device coordinate frame was aligned to coordinate frame of the vehicle: Y-axis to front (longitudinal), X-axis to right (lateral) and Z-axis to up (vertical). The sampling frequency of the inertial sensors were set to 50 Hz and the data was collected from a 40 minute (25 km) drive with 2000 samples of data collected. The collected data was preprocessed to mitigate the noise in the data and to improve the quality of road the roughness classification. With a suitable threshold as the low-pass filter the high-frequency noise were mitigated from the data. After the filtering the triad accelerometer data (x, y, z) and the triad gyroscope data (x', y', z') sample vectors were combined into single magnitudes $m = \sqrt{x^2 + y^2 + z^2}$ and $m' = \sqrt{x'^2 + y'^2 + z'^2}$ respectively. The magnitudes m and m' were buffered into 64 value blocks, $(m_0, ..., m_{64})$ and $(m'_0, ..., m'_{64})$ respectively, representing a segmented sliding window. The computed magnitudes of the time domain variables were converted into frequency domain feature vectors $(f_0, ..., f_{63})$ of Fourier coefficients with Fourier Fast Transform. To each frequency domain feature vector the maximum value of the accelerometer magnitude (MAX_{acc}) sliding window and the gyroscope magnitude (MAX_{gyro}) sliding window were added respectively. Additionally each feature vector was provided with a label *Smooth* or *Potholed*. All the extracted features were analyzed with *Waikato Environment for Knowledge Analysis* (WEKA) [36], a knowledge analysis and machine learning tool. Correlation based Feature Selection method (CFS) of the WEKA tool was used to select the most appropriate features to train the classifier. The CFS assumes that the features have high correlation with the given class but are uncorrelated with each other. 25 features which effectively classify the road roughness were identified with the CFS and selected from the feature vector windows as the training data.

In the *SmartRoadSense* system the data from 3-axis accelerometer and GPS receiver were collected at the frequency of 100 Hz and 1 Hz respectively [3]. Along with accelerometer measurement data location information, bearing, velocity and timestamp were collected. Data from the sensors were collected once per second on average due to the GPS receiver frequency. The data was processed using a sliding window with 100 samples a window with 50 sample overlap. In the *SmartRoadSense* system the road surface profile $w(x)$ was modelled as first order low-pass filtered white Gaussian noise for which the autocorrelation function (ρ_{ww}) is

$$\rho_{ww} = q\delta(x), \tag{4.14}$$

where q is the *power spectral density* (PSD) magnitude and $\delta(x)$ is the *Dirac delta function* [3]. The PSD S_{ww} is obtained by

$$S_{ww}(\Lambda) = q, \tag{4.15}$$

where Λ is the spatial frequency obtained in cycles [3]. The frequency response $H(\Lambda)$ of the first order low-pass filter is

$$H(\Lambda) = \frac{1}{p + j2\pi\Lambda}. \tag{4.16}$$

With Eq. 4.16 the PSD for the road elevation profile $S_{rr}(\Lambda)$ is obtained by

$$S_{rr}(\Lambda) = S_{ww}(\Lambda)\,|H(\Lambda)|^2 = q\left|\frac{1}{p + j2\pi\Lambda}\right|^2. \tag{4.17}$$

Parameter p is the real and j is the imaginary part of a complex number representing the spatial frequency [27]. According to Alessandroni et al the parameters q and p completely characterize the statistical properties of the road profile in the model [3]. By assuming an ideal point that follows the road profile closely has a constant horizontal velocity v. It can be proved with Eq. 4.17 that the continuous time Fourier transform of the vertical acceleration is obtained by

$$A_y(f) = \frac{(j2\pi f)^2}{p + j2\pi f\frac{1}{v}} W(f) \tag{4.18}$$

and this vertical acceleration has the temporal PSD given by

$$S_{A_yA_y}(f) = qv\left|\frac{(j2\pi f)^2}{pv + j2\pi f}\right|^2. \tag{4.19}$$

The function W is Fourier transform of frequency f [27]. With this the road profile characterization parameters p and q in Eq. 4.17 can be obtained by analyzing the PSD of the vertical acceleration according to Alessandroni et al [3]. In the case of a

smartphone with an accelerometer mounted in a vehicle moving along the road differs from that of the ideal point. Many sources of noise effect the PSD obtained from the accelerometer measurements. The accelerometer measurements are sampled at frequency F_s and the result is a discrete time vector of the triaxial components $a_x(n)$, $a_y(n)$ and $a_z(n)$. Some of the noise sources have low spectral content and others have a periodic spectral content. The noise can be mitigated with a *Linear Predictive Coding* (LPC) predictive filter that estimates the current accelerometer sample from the past samples as

$$e\left(n\right) = a\left(n\right) + \sum_{i=1}^{N} \lambda_i a\left(n-i\right), \tag{4.20}$$

where $a(n) \in \{a_x(n), a_y(n), a_z(n)\}$, λ_i with $i = 1, ..., N$ are the LPC coefficients. N is the prediction filter memory length and $e(n)$ is the residual prediction error according to Alessandroni et al [3].

To collect the data in the study by Aleadelat et al the smartphone was assumed to be fixed horizontally on XY-plane and the focus in the study was on the accelerometer measurements obtained from the Z-axis [2]. The mobile application *AndroSensor* for Android platform smartphones was used to collect the accelerometer measurements with 200 Hz sampling rate. The data was collected from 70 gravel roads of different conditions in the Laramie County in Wyoming. RQRG rating survey for the gravel roads was done at same time by the data collectors (driver and the rater). Similarly to the other work reviewed in this thesis also Aleadelat et al had found that the signals obtained from the accelerometer measurements are speed dependent and mixed with noise from different sources such as vehicle suspension system, engine revolutions and tires amongst others. Aleadelat et al make the same notion about acquired signal from the accelerometer measurements for acting as a carrier signal as was made by Seraj et al in [25] that was discussed in Section 4.2.1. Here they also used the same approach of frequency demodulation to mitigate the noise in the signal [2]. For the gravel roads the high-frequency input in the carrier signal represents the road surface and low-frequency represents all the other factors. The frequency demodulation reduces the effect of the low-frequency components in the signal. After the frequency demodulation the discrete wavelet transformation (DWT) was used to further decompose the signal into a series of wavelet functions. With DWT the different frequencies can be discriminated and the power of the signal in the time-domain can be calculated. Power of the signal allows the detection of road anomalies such as potholes. According to Aleadelat et al DWT is more suitable for the analysis of non-stationary signals such as the road surface from a moving vehicle. The DWT was defined as

$$W_\Psi(s,\tau) = \int_{-\infty}^{\infty} X(t)\Psi_{s,\tau}(t)\mathrm{d}t, \tag{4.21}$$

where $W_\Psi(s,\tau)$ is the wavelet transform coefficients [2] and $X(t)$ is the signal obtained from the accelerometer [1]. The higher the obtained coefficient at any specific time is the more energy is present in the signal. Parameters s and τ are continuous related to scale and translation respectively. $\Psi_{s,\tau}(t)$ is the wavelet transform analyzing function for DWT defined as

$$\Psi_{s,\tau}(t) = \frac{1}{\sqrt{s}}\Psi\Big(\frac{t-\tau}{s}\Big), \tag{4.22}$$

where $s = 2^j$ and $\tau = k * 2^j$ [2]. Integer j is the level of decomposition and integer k is a value from $-\infty$ to ∞. According to Aleadelat there is no defined procedure for choosing the most suitable wavelet family for the DWT. On trial and error basis Sym6 wavelet from the Symlet family was selected with 5 levels of decomposition were used to perform the DWT. The more levels used results in the signal to be decomposed to more finer bands and allows to discriminate better between the sources of noise in the signal. After DWT decomposition the signals were examined to detect road anomalies and correlation between RQRG ratings and DWT coefficients were established.

4.3.2 Detection method computation

With the training data the *C4.5 Decision Tree*, SVM and *Naive Bayes* classifiers were trained to evaluate and select the best performing classifier for the RoadSense system [4]. The classifier with highest accuracy (*C4.5 Decision Tree*) was selected to be used as the prediction model in the mobile application of the RoadSense system. In the prediction phase the real-time measurements from the accelerometer and the gyroscope are filtered and preprocessed similarly like in the training phase apart from labelling (Fig. 4.4). The label is predicted to each of the feature vectors by the *C4.5 Decision Tree* classifier that was trained in the training phase. The RoadSense Android application showed the location trace of the road with the predicted road roughness class on a map.

The accelerometer measurements in the *SmartRoadSense* system were split into segments of the length of M where M is large enough for accurate estimation of the prediction filter and small enough to capture stationary signal in the measurement data samples [3]. *Levinson-Durbin recursion* (Table 4.7) was used to compute the prediction filter for a segment. As previously mentioned in Section 4.3.1 the statistical properties of the road profile model used in the *SmartRoadSense* system are described by parameters q and p. According to Alessandroni et al the information on the parameter q is maintained by the prediction error $e(n)$ but the information on the parameter p is lost due to the whitening produced by the prediction filter [3]. Parameter q is a proportionality parameter in the PSD and a parameter proportional to parameter q

Table 4.7: Pseudo-code for Levinson-Durbin recursion in Matlab notation [3].

```
k = R(2) / R(1);
λ = k;
E = (1 - k^2) * R(1);
for i = 2 : N
  k = (R(i + 1) - λ * R(2 : i)) / E;
  λ = [k, λ - k * λ(i - 1 : -1 : 1)];
  E = (1 - k^2) * E;
end
```

R(0), R(1), ..., R(N) is the autocorrelation sequence on $a(n)$ estimated over a segment.
$\lambda = [\lambda_1, \lambda_2, ..., \lambda_N]^T$ is the prediction filter coefficient vector.

can be inferred by estimating the power of the prediction error P_{P_E} of the segments, defined as

$$P_{P_E} = \frac{1}{M} \sum_{n=1}^{M-1} e\,(n)^2\,. \tag{4.23}$$

The road roughness index, R_I, is inferred by averaging the P_{P_E} of the three accelerometer components is defined as

$$R_I = \frac{1}{3}\left(P_{P_{E_X}} + P_{P_{E_Y}} + P_{P_{E_Z}}\right). \tag{4.24}$$

The mobile application of the *SmartRoadSense* system gathers the data from the sensors and computes the P_{P_E} in real-time. Each P_{P_E} result is computed from 100 data samples which are gathered on average from 100 seconds of data. The results obtained from the accelerometer data are sent to backend server for aggregation and to be visualized on the map of the user interface.

For the finding the RWRG regression model Aleadelat et al extracted the accelerometer data from a smartphone and analyzed the data in MATLAB by performing the frequency demodulation and DWT [2]. By experimenting with the frequency demodulation the frequency 98 Hz was found to represent the carrier signal. The frequency demodulation was noticed to well isolate the carrier signal from the unwanted components and the resulting signal clearly indicating the sections with road anomalies and smooth road sections. DWT analysis was performed on the demodulated signal to better characterize the signal from the road anomalies. With experiments the 3^{rd} level of DWT coefficients was found to represent the road conditions the best. The magnitude of the DWT coefficients was considered to identify the severity of the road anomalies. The higher the coefficient correlated tot higher severity of the road anomaly according to Aleadelat et al [2]. By comparing the different overall RQRG ratings between 1-9 with the collected road profile data the value 2.5 (absolute value of 3^{rd} level

coefficient) was determined as a threshold between normal (<= 2.5) and anomalous (> 2.5) road. By analysing the data the severe washbords and potholes can be detected but further investigation is required to associate between the severity of the road anomalies and the measured signal according to Aleadelat et al [3]. To evaluate the predictability of the RQRG ratings from the smartphone accelerometer measurements an explanatory variable, the sum of local maxima points (SLM) of the absolute coefficient values, was found to correlate well enough. The RQRG rating prediction model is defined as

$$RQRG = 7.5e^{-0.003*SLM} \quad ; \quad R^2 = 0.78. \tag{4.25}$$

4.3.3 Performance evaluation of the methods

Allouch et al performed analytical validation to evaluate the performance of the *C4.5 Decision Tree*, *SVM* and *Naive Bayes* classification algorithms (WEKA CFS) to classify the road roughness [4]. 10-fold cross-validation validation was performed for each of the classifiers. $ROCArea$ and the following measures were calculated to evaluate the classifier's performance:

$$Accuracy = \frac{(TP + TN)}{(TP + TN + FP + FN)}, \tag{4.26}$$

$$TPRate = \frac{TP}{(TP + FN)}, \tag{4.27}$$

$$FPRate = \frac{FP}{(FP + TN)}, \tag{4.28}$$

$$Precision = \frac{TP}{(TP + FP)}, \tag{4.29}$$

$$Recall = \frac{TP}{(TP + FN)}, \tag{4.30}$$

$$Recall = \frac{2 \times Precision \times Recall}{(Precision + Recall)}, \tag{4.31}$$

where TP is the true-positives count, TN is the true-negatives count, FP is the false-positives count and FN is the false-negatives count. The performance evaluation results are presented in Table 4.8. Based on the results *C4.5 Decision Tree* classifier is the most accurate classier with the average accuracy of 98.5 % and the average

Table 4.8: Performance comparison of three algorithms using different metrics [4].

Classifier	Accuracy	TPR	FPR	Precision	Recall	F-Measure	ROC
C4.5	98.50 %	0.985	0.064	0.985	0.985	0.985	0.987
SVM	95.25 %	0.953	0.265	0.951	0.953	0.950	0.844
Naive Bayes	96.90 %	0.969	0.049	0.972	0.969	0.970	0.976

F-measure of 0.985. Allouch et al analysed also the impact of the sensor data with the *C4.5 Decision Tree* and concluded that using only gyroscope measurements the overall accuracy of the *C4.5 Decision Tree* classifier was better ($\sim$ 98 %) than with only accelerometer measurements ($\sim$ 97 %).

For experimenting with *SmartRoadSense* Motorola Moto G smartphones were installed in two public buses and used to collect the data [3]. 215 300 data points from 744 different roads with the length of 275 089 meters were collected over two weeks. From the collected data road roughness indexes were appropriately processed and sent by the app and server aggregated the results for the user interface map visualizations. The aggregated results were shown on the map with equidistant dots with colours ranging from green to red. The greenish coloured points represented smooth and reddish coloured points represented rough.

According to Aleadelat et al the relationship between the RQRG ratings and SLM explains 78 % of the variation in the predicted ratings [2]. The prediction model was validated by collecting data from 35 new gravel roads and rating them with RQRG rating survey. Then the RQRG predictions were computed with the Equation 4.25 and the prediction results showed good agreement with the RQRG rating survey results. Equation 4.25 provided reasonable prediction for 77 % of the RQRG survey ratings. Paired t-test result had the difference of less than 1.3 units between the predictions and the actual RQRG survey ratings was not significant at 95 % confidence level.

4.4 Detecting driving maneuvers

In this section the detection of the driving maneuvers are discussed. Singh, Juneja and Kapoor show that different driving maneuvers executed by the driver of a vehicle are reflected in the accelerometer measurements of a smartphone [26]. Mobile application for Android platform smartphones was implemented to collect and to annotate the ground truth for different driving maneuvers. The accelerometer measurements were collected and analyzed to observe the characteristics of the different driving maneuvers. It is assumed that the smartphone device coordinate frame is aligned with the vehicle's coordinate frame with lateral x-axis pointing to right, longitudinal y-axis pointing

forward and vertical z-axis pointing upwards. Singh et al used the following characterization for the driving maneuver reflections [26]. The *Left Turn* is characterized by abrupt decrease in the x-axis acceleration. The *Left Lane Change* is characterized by the initial decrease followed by incrementation back to normal in the x-axis acceleration. With the aforementioned descriptions of maneuver reflections it is assumed that there is an error in [26] and the *Right Turn* is characterized by abrupt increase in the x-axis acceleration. The *Right Lane Change* is characterized by the initial increase followed by decrementation back to normal in the x-axis acceleration. The *Sudden Breaking* is characterized by abrupt decrease followed by the increase back to normal level in the y-axis acceleration and continuing with almost a straight-line. It is assumed that the straight-line is there only if the vehicle was breaking to full-stop. The *Sudden Acceleration* is characterized by abrupt increase in the y-axis acceleration. In both *Sudden Breaking* and *Sudden Acceleration* x-axis and y-axis register the changes in acceleration forces due to the abrupt jolts. It is assumed that these jolts are only experienced depending on the intensity of the sudden maneuvers. As the different driving maneuvers are detectable (and can be annotated) from the acceleration measurements it is concluded that they can be classified with a suitable classifier trained with suitable amount of collected training data or with a customized threshold-based filtering sequence.

In another method *Dynamic Time Warping* algorithm is used to detect the driving maneuvers from a smartphone embedded inertial sensor measurements. Johnson and Trivedi proposed the *MIROAD* system which uses smartphone based sensor-fusion and Dynamic Time Warping (DTW) to detect potentially-aggressive driving behaviour from the embedded sensor measurements reflected from the driving maneuvers [17]. The *MIROAD* system was designed to run solely on a mobile device without the requirement to use any external hardware. For driving maneuver detection a simple algorithm like DTW was assumed as sufficient instead of labelling a large number of samples due to the limited range of vehicle movement capabilities. The *MIROAD* system uses the smartphone embedded sensor measurements of the accelerometer, gyroscope and the magnetometer to detect the different driving maneuvers. The gyroscope measurements were assumed indicate the vehicle movement better than the accelerometer measurements by Johnson et al [17]. The correction with respect to the gravity from the accelerometer and the correction with respect to magnetic north from the magnetometer were used in conjunction with the rotation measures of the gyroscope to obtain more accurate device orientation. This procedure allows the *MIROAD* system to find the Euler rotations from a reference orientation more accurately. The driving maneuver detection in the *MIROAD* system is divided into the categories of lateral T (Eq. 4.32) and longitudinal L (Eq. 4.33) movements. The sensor measurements consists

of the gyroscope measurements $G = \{g_x, g_y, g_z\}$ in rad/s, the accelerometer measurements $A = \{a_x, a_y, a_z\}$ in m/s^2 and the device Euler angle rotations $E = \{e_x, e_y, e_z\}$ in radians from the reference orientation R. The category T contains gyroscope measurements g_x as the turns are best observed from the x-axis rotations in the *MIROAD* system and the accelerometer measurements a_y and Euler angle rotations e_x describe the device orientation to improve the detecting accuracy.

$$T = \{g_x, a_y, e_x\} \tag{4.32}$$

$$L = \{g_y, a_z\} \tag{4.33}$$

Along with the category T the pure gyroscope measurements G and the accelerometer measurements A were evaluated with the DTW algorithm to detect the driving maneuvers [17]. The types of driving maneuvers detected by the *MIROAD* system were right turns (90°), left turns (90°), U-turns (180°), aggressive right turns (90°), aggressive left turns (90°), aggressive U-turns (180°), aggressive acceleration, aggressive braking, swerve right (aggressive lane change), swerve left (aggressive lane change), device removal and excessive speed. Normal lane change maneuvers do not create enough acceleration or rotation to be detected from the noise according to Johnson et al [17]. Also a device removal, excessive speed, acceleration, braking and the longitudinal events L were not in focus of the study for the DTW as they are easy to detect by using thresholds.

4.4.1 Collecting and preprocessing the raw data

The *MIROAD* system was developed for iPhone 4 device and the accelerometer, gyroscope and the device orientation data were sampled at the rate of 25 Hz [17]. Similar set up can be implemented for the Android platform smartphones. The orientation of the device is assumed to be fixed in landscape orientation with z-axis pointing to back of the vehicle, y-axis pointing to the right and x-axis pointing to upwards. The collected sensor measurements contain noise and a low-pass filter is used to mitigate the additional noise from the sensor measurements.

In order to classify the different driving maneuvers the *MIROAD* system determines when the driving maneuver event starts and when it ends. The starting point is detected by computing simple moving average (SMA Eq. 4.34) for the rotational energy of the x-axis with the window size k of the i^{th} sample [17].

$$SMA = \frac{g_x(i)^2 + g_x(i-1)^2 + \cdots + g_x(i-k-1)^2}{k} \tag{4.34}$$

If the SMA exceeds the upper threshold t_U then the driving maneuver event begins at $g_x(i-k-1)$ and ends when the SMA of the concatenated subsequent samples is less then the lower threshold t_L [17]. The driving maneuver event is discarded if the event length exceeds 15 seconds. For the detection with the DTW algorithm a set of 120 templates totalling 40 driving maneuvers from the three sensor measurement sets were created.

4.4.2 Detection method computation

According to Johnson et al the DTW algorithm considers a $m \times n$ grid based on the vector $X = \{x1, x1, ..., xi, ..., xm\}$ and the vector $Y = \{y1, y1, ..., yi, ..., yn\}$ on the left and on bottom side of the grid respectively[17]. In the grid each cell represents the euclidian distance $D(i, j)$ between each of the vector elements as

$$D(i, j) = \|x_i - y_j\|. \tag{4.35}$$

The DTW algorithm finds the optimal alignment of the vectors X and Y [17]. In the *MIROAD* system the detected driving maneuver event vector is aligned with the pre-recorded template vectors which represent the driving maneuvers to be detected. The optimal warping path p between the vector elements is found with the $D(i, j)$ (Eq. 4.35) for each alignment. The sum of the path p is the total cost c_p of the alignment path (Eq. 4.36). The lowest path cost c_p designates the closest matching template maneuver.

$$c_p(X, Y) := \sum_{k=1}^{K} c(x_{mk}, y_{nk}) \tag{4.36}$$

4.4.3 Performance evaluation of the methods

The results of the evaluation experiments of the DTW algorithm to detect the different driving maneuvers with A, G and T sensor data are presented in Table 4.9. According to Johnson et al 201 driving maneuvers were collected for the evaluation from which 50 driving maneuvers were considered potentially-aggressive [17]. The driving maneuvers considered in the table are right turn (R), left turn (L), U-turns (U), aggressive right turn (HR), aggressive left turn (HL), aggressive U-turn (HU), swerve right (SR) and swerve left (SL). The results show that by using only accelerometer or gyroscope measurements the DTW has some difficulties in detecting some of the driving maneuvers as compared to using a combined sensor measurement set.

Table 4.9: Recognition rate (%) comparison for A, G and T measurements [17].

	R	**L**	**U**	**HR**	**HL**	**HU**	**SR**	**SL**	**Total**
A	72	68	23	71	100	100	100	83	77
G	76	63	46	71	100	100	100	83	79
T	92	83	77	100	100	100	100	83	91

4.5 Detecting the vehicle speed

In this section a method to obtain the accurate vehicle speed is discussed. In smartphones the speed of travel is reliably obtained with the GPS receiver when in open areas but the speed might be unobtainable when the GPS signal is blocked in urban canyons or by the trees with foliage on the forest roads. Han, Jiadi, Hongzi, Yingying, Jie, Yanmin, Guantao and Minglu proposed the *SenSpeed* system to accurately estimate the vehicle speed from the smartphone accelerometer measurements [15]. To obtain the estimation of speed the smartphone accelerometer measurements along the vehicle's moving direction are integrated over time. With the proposed system the solutions to the recognized problems with noisy acceleration measurements, estimation accuracy and real-timeliness are provided. Han et al found that regardless of the smartphone type the integration results over the acceleration measurements deviate a lot from the true speed of the vehicle and that the error increases almost linearly over time [15]. Based on this observation they suggested that as the changes of acceleration error over time are small the error can be corrected with deriving speed error estimates at some time points. The smartphone embedded inertial sensors (accelerometer and gyroscope) are used to detect the natural driving conditions (*reference points*) with features from which the vehicle speed can be inferred. Reference points are used to eliminate the acceleration errors and to accurately estimate the real-time vehicle speed. The natural driving conditions of making turns, stopping and driving on uneven road surfaces are considered as the reference points in *SenSpeed*.

4.5.1 Collecting and preprocessing the raw data

Figure 4.5 illustrates the workflow of the *SenSpeed* system [15]. Accelerometer and gyroscope sensor measurements obtained continuously from the smartphone embedded inertial sensors are used to estimate the vehicle speed. As the smartphone device can be in arbitrary position the device's coordinate frame need to be aligned with the vehicle's coordinate system. The alignment is done in *Coordinate Reorientation* step in which the sensors' measurements are aligned with the vehicle's coordinate system. The alignment is done with a rotation matrix $R = \left[\hat{i}\ \hat{j}\ \hat{k}\right]$, where $\hat{i}$, $\hat{j}$ and $\hat{k}$ are the

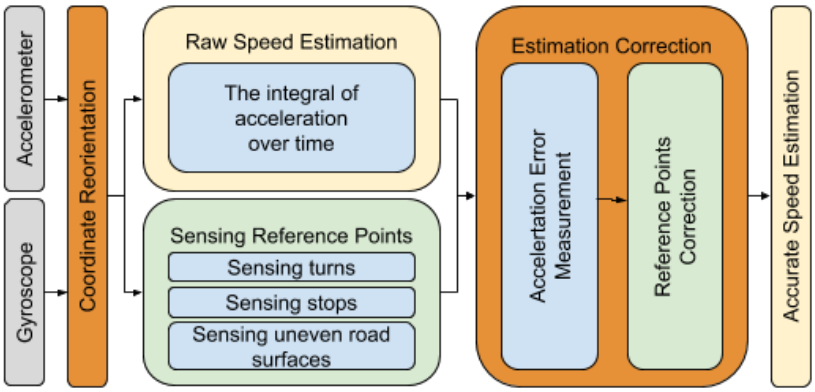

Figure 4.5: The system architecture of *SenSpeed* [15].

three-dimensional coordinate vectors of the device's coordinate frame x, y and z axes to direction of the vehicle coordinate frame [15]. The vectors in the rotation matrix are the measurements obtained from the accelerometer and the gyroscope. The z-axis vector in the rotation matrix is recalibrated by $\hat{k} = \hat{i} \times \hat{j}$ to keep the vectors in the rotation matrix in orthogonal orientation.

4.5.2 Detection method computation

In *Raw Speed Estimation* (Fig. 4.5) step the raw speeds are obtained from the aligned accelerometer measurements. It is assumed by Han et al that the y-axis is aligned with the vehicles Y-axis and is to the direction of acceleration of the vehicle [15]. The vehicle speed can obtained with the integral of the acceleration over time as

$$Speed\,(T) = Speed\,(0) + \int_0^T acc\,(t)\,\mathrm{d}t, \tag{4.37}$$

where *Speed* is the vehicle speed at time T and $acc\,(t)$ is the vehicles acceleration function of each time instant t [15]. Since the accelerometer in practice produces a series of acceleration samples with the chosen sampling rate, instead of using the Eq. 4.37, the speed can be obtained with

$$Speed\,(T) = Speed\,(0) + \sum_{i=0}^{T \cdot k} acc_y\,(i)\,, \tag{4.38}$$

where k is the chosen sampling rate and $acc_y\,(i)$ is the i^{th} sample of the aligned y-axis measurement [15]. The gyroscope measurements are monitored continuously by the *SenSpeed* system to detect the changes in the smartphone's orientation in order to re-calculate the rotation matrix. In *Sensing Reference Points* step the aligned accelerometer and gyroscope measurements are used to detect the *reference points* and to calculate the vehicle speed at each detect *turn*, *stop* or *uneven road surface*. The centripetal force experienced when vehicle turns, is related to vehicles speed, angular

velocity and turning radius and the tangential speed of a turning vehicle can be derived from the acceleration and gyroscope measurements. From $\nu = \omega\Re$, $a = \omega^2\Re$ and $\omega = \omega'$ where a is the centripetal acceleration, ω' is the angular velocity of the vehicle, $\Re$ is the turning radius and ω is the angular velocity related to the center of the orbit the following equation can be obtained

$$\nu = \frac{a}{\omega'}. \tag{4.39}$$

According to Han et al the speed ν can obtained with the Eq 4.39 where the centripetal acceleration a can be obtained from the accelerometer measurements and the angular velocity ω can be obtained from the gyroscope measurements [15]. The speed at the *turn* reference point obtained with the Eq 4.39 together with the angular velocity changes obtained from the gyroscope and the speed obtained from the vehicle through OBD-II adapter were analyzed by Han et al to see that there clearly is a change of angular velocity when making a turn. The *SenSpeed* system uses a trained threshold to determine a vehicle turn from the gyroscope measurements. The speed obtained with the Eq. 4.39 also seemed to be very close to the ground truth obtained with ODB-II adapter. With experiments the speed measurement error was observed to be lower than 2.2 mph in 80 % of the time with the average error of 1.1 mph, with the accuracy decreasing as the speed increases. The *stop* reference points are obtained when the vehicle speed decreases to zero. With the accelerometer measurements the stop is noticed when the standard deviation of the aligned z-axis values remains low. With this the vehicle speed is zero at detected stops. The *uneven road surface* is detected from the aligned accelerometer measurements. The vehicle speed ν at these reference points can be measured with

$$\nu = \frac{W}{\Delta T}, \tag{4.40}$$

where ΔT is the time interval between the two peaks caused by the front wheel axel and the back wheel axel experiencing the same disruption in the road surface, and W is the wheelbase of the vehicle [15]. Auto-correlation analysis is used to find ΔT based on the similarity of the two peaks. Auto-correlation R of the time lag τ is obtained by

$$R(\tau) = \frac{E\left[(Acc_i - \mu)\left(Acc_{i+\tau} - \mu\right)\right]}{\sigma^2}, \tag{4.41}$$

where μ is the mean value of the z-axis accelerometer measurements Acc and σ is the standard deviation [15]. To obtain ΔT another maximum peak needs to be found besides the peak at $\tau = 0$. The distance between the second maximum peak and $\tau = 0$ is equal to ΔT. W can be obtained from vehicle's specification or to minimize the user involvement, after ΔT is obtained W can be obtained with

$$W = \nu \cdot \Delta T, \tag{4.42}$$

where ν is using the vehicle speed estimated between the reference points obtained earlier [15]. The accuracy of the speed measurement at uneven road surface reference points achieved the measurement error lower than 1.7 mph in 80 % of the time at speeds 0 - 30 mph. Measurement error lower than 2.2 mph in 80 % of the time at speeds 60 - 90 mph. The average measurement error was 1.12 mph. In the *Estimation Correction* step the raw speed estimations are corrected with the acceleration error estimates between two adjacent reference points. The error of the speed estimate at each reference point a and b are $\Delta S\left(T_a\right) = S\left(T_a\right) - RPS_a$ and $\Delta S\left(T_b\right) = S\left(T_b\right) - RPS_b$, where T is the time vehicle passed the reference point and RPS is the measured reference point speed. As the acceleration error is observed to be nearly constant and closely related to $\Delta S\left(t\right)$ curve, the acceleration error between the points a and b can be calculated with

$$\tilde{A} = \frac{\Delta S\left(T_b\right) - \Delta S\left(T_a\right)}{\Delta T_a^b}, \tag{4.43}$$

where ΔT_a^b is the time interval between the points a and b [15]. The accumulative error according to Han et al from T_a to t is $\int_{T_a}^{t} \tilde{A}\ \mathrm{d}t$ i.e. $\tilde{A} \times \left(t - T_a\right)$ [15]. The corrected speed estimation $S'\left(t\right)$ between the points a and b is obtained with

$$S'\left(t\right) = S\left(t\right) - \Delta S\left(T_a\right) - \tilde{A} \times \left(t - T_a\right), \tag{4.44}$$

where $S\left(t\right)$ is the integral of the aligned y-axis accelerometer measurements from zero to time t [15]. To correct the speed estimation between two adjacent reference points the Eq. 4.38 requires the information from those two reference points. Therefore the Eq. 4.44 (*offline estimation*) can not be used for the speed estimation in real-time since no information is available of the next reference point. As the acceleration error change over time is known to be small, the current acceleration error can be inferred from the most recent reference points by using *exponential moving average*. According to Han et al the current acceleration error $\tilde{A}_i$ between the reference points i and $i+1$ is updated with Eq. 4.45 once the i^{th} reference point is detected.

$$\tilde{A}_i = \alpha \cdot \tilde{A}_{i+1} + \left(1 - \alpha\right) \times \frac{\Delta S\left(T_i\right) - \Delta S\left(T_{i-1}\right)}{\Delta T_{i-1}^i}, \tag{4.45}$$

where α is the weight coefficient. The correction of the real-time speed estimation $S'\left(t\right)$ (*online estimation*) between reference points i and $i+1$ is obtained with

$$S'\left(t\right) = S\left(t\right) - \Delta S\left(T_i\right) - \tilde{A}_{i+1} \times \left(t - T_i\right). \tag{4.46}$$

4.5.3 Performance evaluation of the methods

The accuracy of the speed estimate is depended on the density of the detected reference points [15]. The effect of the reference point density was analyzed with data collected

from two different road types (streets and highways) from two different cities. Data was collected over 1500 miles driving in one month in Shanghai and 1000 miles of driving in three weeks in New York City. The *SenSpeed* system detected from the data about 9 rps/mile (reference points per mile) on streets and 5 rps/mile on highways from the Shanghai data. Respectively from the New York City data the *SenSpeed* system detected 11 rps/mile on streets and 9 rps/mile on highways. As the overall performance when all reference points and road types were considered the *SenSpeed* system achieved better accuracy in the speed estimation compared to GPS speed estimation. On New York City (Manhattan) streets the average error for the speed *offline estimation* was 0.7 mph and 1.3 mph for the speed *online estimation*, and when compared to the GPS speed estimation with 2.8 mph and 3.1 mph error respectively. When evaluating the speed estimation accuracy with different density levels of reference points (i.e. 25 %, 50 %, 75 %, 100 %) the accuracy of the speed *offline estimation* is always high regardless of the density level. With the *offline estimation* the error is lower than 1.2 mph for 80 % of the time if 100 % density level is used and there is no obvious change in the accuracy if the reference points are reduced to 25 %. With the *online estimation* the error is lower than 2.3 mph of 80 % of the time if 100 % density level is used and there is no obvious change in the accuracy if reference points are reduced to 50 %. When density level is reduced to 25 % the estimation error is still lower than 2.3 mph for 65 % of the time. Han et al conclude that the speed *online estimation* is still robust in urban environments even with the declination of the reference point density and has potential to be employed in rural areas [15].

4.6 Detecting bridge condition

In this section two approaches for monitoring bridge condition are discussed. The approaches consider the use of smartphone embedded sensor data obtained from a vehicle moving on a bridge. In both of the approaches the STRIDEX algorithm is utilized to infer the necessary information from the obtained noisy smartphone sensor data for monitoring bridge structural condition.

Matarazzo, Vazifeh, Pakzad, Santi and Ratti suggest the use of smartphone sensor data in the structural health monitoring (SHM) of bridges [19]. The bridge vibration data for the structural health monitoring is primarily obtained with the use of a sophisticated sensor network of fixed sensor nodes on the bridge being monitored. As the alternative a mobile sensor network have been recently suggested for collecting the data. The use of smartphones with embedded sensors as the nodes of such mobile sensor network has been studied by Matarazzo et al [19]. Crowdsourcing of sensor data from a mobile sensor network of smartphones would allow the structural health

monitoring of bridges with no fixed sensor network in place. The idea is to initially create a baseline conditions for a healthy structure of an individual bridge and start to collect data of the structural features obtained from a mobile sensor network data. After collecting the data statistical tests could be conducted to compare and to identify statistically significant values which could indicate a change in the structural condition of a bridge.

In a study Eshkevari and Pakdaz propose a structural identification (Fig. 4.6) approach to extract the mechanical properties of the dynamic systems such as bridges [12]. For the proposed structural identification approach was the *Second Order Blind Identification* (SOBI) algorithm for separating the sources of a mobile sensor measurements collected from the vehicles moving on top of a bridge. Eshkevari et al assume that the mobile sensor acceleration measurements are a mixture of two main sources of vibrations generated from the road surface roughness over the bridge and the dynamic accelerations from the bridge structure [12]. In order to get a valid input for the structural system identification algorithm (STRIDEX) a blind source separation (BSS) of the mixed data should be performed. SOBI is one of the most used algorithms for BBS along with Independent Component Analysis (ICA) in civil engineering. The mixed data of structural dynamic responses the order of the samples is significant which is a property not taken in consideration in the ICA algorithm. In this respect the SOBI algorithm is assumed more suitable for the mixed data with the sources of different spectral variations and it is also computationally less expensive as it considers only no higher than second order independencies [12].

4.6.1 Collecting and preprocessing the raw data

Based on the vast number of smartphone users and the existence of crowdsensing mobile applications for smartphones Matarazzo et al suggest the concept of crowdsourcing to collect the bridge vibration data for bridge health monitoring [19]. It is assumed that the sensor data from the mobile sensor network of smartphones in vehicles could be collected during the daily traffic of the vehicles on the bridge. The vibrations of the vehicle, the bridge and their interactions are assumed to be reflected on the mobile sensor data. According to Matarazzo et al in case of the fixed sensor networks mainly the state-space approaches are used to analyze the sensor data and to extract the structural features from dynamic systems such as the bridges [19]. The mobile sensor network data from a structural system is classified as dynamic sensor network (DSN) data and it can be modelled as the truncated physical state-space model (TPM). The state equation (Eq. 4.47) and the observation equation (Eq. 4.48) describe the TPM

[19, 12].

$$x_k = Ax_{k-1} + \eta_k \tag{4.47}$$

$$y_k = \Omega_k C x_k + \nu_k \tag{4.48}$$

The discrete-time state variables x_k contain the structural responses at each time-step k for a set of points in space [19]. The observation variables y_k contain the data from the DSN at each time-step k with a changing locations over time. A is the discrete-time state matrix that specifies how the states behave over time. Ω_k is the mode shape regression term at time-step k and C is the discrete-time observation matrix. The product $\Omega_k C$ relates the observations with the states. Parameter η_k is the stochastic state input at time-step k, which can be assumed as random if not measured. Parameter ν_k is the stochastic measurement error at time-step k which is often assumed as Gaussian noise [19].

Eshkevari et al used a numerical model of a bridge to simulate the mobile sensor measurements to contain the structural dynamic responses and the road roughness [12]. The simulated data was used to experiment the performance of the SOBI algorithm to find both the roughness-based vibrations and the dynamic acceleration response vibrations of the bridge structures. The separated dynamic responses were used as input for the STRIDEX algorithm to find the natural frequencies and the mode shape. Figure 4.6 illustrates a flow chart of the proposed identification algorithm.

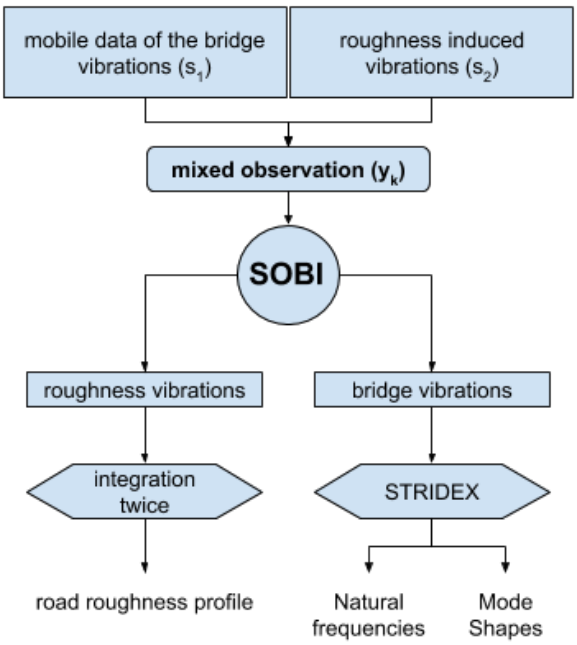

Figure 4.6: Flow-chart of the proposed identification algorithm [12].

In the application of SOBI algorithm Eshkevaeri et al assumed that the smartphones with the embedded accelerometer sensor were attached to a rigid vehicle and the mixed road surface roughness and bridge dynamics measurements were not convoluted [12]. With this assumption the mixed signal with noise can be expressed as

$$x_i(t) = \sum_{j=1}^{n} a_{ij} s_j(t) + \sigma_i(t), \qquad i = 1, 2, ..., n \tag{4.49}$$

and expressed in a matrix notation as

$$x(t) = As(t) + \sigma(t) = y(t) + \sigma(t), \tag{4.50}$$

where A is the mixture matrix and is assumed to be an unknown constant matrix that is estimated from the observations [12]. Parameter $\sigma(t)$ is an uncorrelated noise vector. Parameter $s(t)$ is a vector of the source measurements at time-step t. Parameter $x(t)$ is the observation of the mixed measurements. The source measurements are commonly assumed to be unit variance random processes, so $E[s_i^2(t)] = 1$ for $i = 1, 2, ..., n$. With stationary, uncorrelated and unit variance sources the obtained covariance matrix is

$$R_s(0) = E[s(t)\, s^*(t)] = I, \tag{4.51}$$

where $s^*(t)$ is the conjugate transpose of the vector $s(t)$ [12]. With Equation 4.50 and the additive noise vector that is uncorrelated and independent to the sources the result is

$$R_x(0) = E[x(t)\, x^*(t)] = E\left[As(t)\, s^*(t)\, A^H\right] + E[\sigma(t)\, \sigma^*(t)] = AA^H + \sigma^2 I. \tag{4.52}$$

According to Eshkevari et al the SOBI algorithm has two steps [12]. The first step is whitening, for which a linear transformation W is calculated as $E\left[Wy(t)\, y^*(t)\, W^H\right] = I$. The covariance matrix of noisy observation gives $E[yy^*] = AA^*$. With this the result is

$$E\left[Wyy^*W^H\right] = WAA^HW^H = I = UU^H. \tag{4.53}$$

With the whitening matrix W a unitary matrix U such that $U = WA$ can be found [12]. The actual observation x (note, not y) is noisy, therefore if $z(t) = Wx(t)$ it follows that

$$E[zz^*] = E\left[Wxx^*W^H\right] = WR_x(0)\, W^H. \tag{4.54}$$

In the second step the unitary matrix U is determined with the time-lagged observation covariance matrix as

$$\begin{aligned} R_z^w(\tau) &= E[z(t+\tau)\, z^*(t)] \\ &= WE[x(t+\tau)\, x^*(t)]\, W^H \\ &= WAE[s(t+\tau)\, s^*(t)]\, A^HW^H, \qquad \forall\, \tau \neq 0, \end{aligned} \tag{4.55}$$

from which $R_z^w(\tau) = UR_s(\tau)U^H$ is obtained [12]. According to Eshkevari et al the idea is to find a unitary matrix U that diagonalizes any whitened covariance matrix $R_z^w(\tau)$. Such matrix is determined by decomposing the time-lagged covariance matrix of the whitened observation $R_z^w(\tau)$. Accordingly A is found from $U = WA$ and the sources as $x(t) = As(t)$ completing the SOBI algorithm. The separated source for bridge vibration is processed with STRIDEX algorithm to extract the modal properties.

4.6.2 Detection method computation

STRIDE algorithm is a state space based procedure for structural identification by using expectation maximization [12]. According to Eshkevari et al in STRIDE algorithm expectation maximization is used iteratively to maximize the unobserved state vectors estimate and the unknown state-space matrices. In the maximization step the STRIDE algorithm defines a superparameter to contain of all state space unknowns and by assuming a given set of unobserved state the STRIDE algorithm maximizes the log-likelihood of the state space. In the expectation step the STRIDE algorithm uses Kalman Filter and Rauch-Tung-Striebel smoother on the input data to estimate the unobserved states. As an asymptotically converging algorithm the STRIDE algorithm finds a local maximum for which the initialization of the superparameter is crucial. According to Eshkevari et al STRIDEX is an upgraded version of the STRIDE for the mobile sensing networks in which the position of the mobile sensors are known at each step [12].

4.6.3 Performance evaluation of the methods

According to Matarazzo et al STRIDEX algorithm and mobile sensor network data have been simulated in laboratory to perform on the level set by the standards of the fixed-sensor system identification (SID) methods and the adaptation of mobile sensors for SHM is expected to grow [19]. According to Eshkevari et al the evaluation was based on the numerically modelled bridge and the mixed observations were simulated [12]. With the input data obtained with the SOBI algorithm the STRIDEX algorithm is able to identify the fundamental modes, and estimate the natural frequencies and mode shapes. The algorithm identified fairly well the values for Rayleigh damping ratios that were preset for the evaluation according to Eshkevari et al [12]. The first mode and its corresponding attributes were not effectively identified.

5. Summary and future work

This chapter provides a summary of the literature review done in the previous Chapter 3 and Chapter 4 of this thesis. Also two topics for potential future analysis are presented. In Section 5.1 the previously introduced road condition factors and road anomalies are summarized together with the computational road anomaly detection methods to find out the appropriateness for each of the road anomalies. Section 5.2 outlines a potential research topic for generating training data based on any already existing ground truth data of normal roads and different road anomalies. Section 5.3 outlines another potential research topic for predicting the future road data to infer the predicted road conditions.

5.1 Review summary

The road condition factors and the respective road anomalies presented in Section 3.2 are summarized in the Table 5.1. The expected phenomenas and their reflections in the sensor measurements about the road condition factors and the road anomalies discussed in Section 3.2 are based on the analysis done by the author of this thesis. The suggested methods to detect a road anomaly is based on the analysis of the reviewed literature of the methods discussed in Chapter 4.

As can be seen from the Table 5.1 several of the condition factors with the respective road anomalies are expected to produce very similar kind of phenomenas (e.g. in case of Road bearing & structural deficiencies and Dewatering). This similarity makes it difficult to separate the actual underlaying condition factor, or even the road anomaly in some cases, from one another based on the phenomenas and the sensor measurements. The reviewed literature gives background for the assumptions made in this thesis that the different road anomalies can be identified based on their basic characteristics reflected in the sensor measurements. The column *Suggested methods* presents the suggestions made by the author of this thesis as the appropriate computational methods for detecting the corresponding road anomaly.

Table 5.1: Summary of road condition factors with the assumed implications.

Condition factor	Road anomaly	Expected phenomena	Axes and detecting sensor	Suggested methods
Road bearing & structural deficiencies	road softness	speed deceleration	y-axis accelerometer GPS	senspeed threshold-mod
	rutting	orientation peaks acceleration peaks	z-axis gyroscope x-axis accelerometer y-axis accelerometer	svm-multi c4.5 threshold-mod miroad
	collapsed road	orientation peaks acceleration peaks	x-axis gyroscope y-axis gyroscope z-axis accelerometer	threshold svm c4.5
Dewatering	road softness	speed deceleration	y-axis accelerometer GPS	senspeed threshold-mod
	rutting	orientation peaks acceleration peaks	z-axis gyroscope x-axis accelerometer y-axis accelerometer	svm-multi c4.5 threshold-mod miroad
	potholes, bumps	acceleration peaks orientation peaks	z-axis accelerometer x-axis gyroscope y-axis gyroscope	threshold svm c4.5
Wearing course	surface roughness	steady vibration levels	z-axis accelerometer x-axis gyroscope y-axis gyroscope	threshold svm c4.5 lpc rqrg sobi
		speed deceleration	y-axis accelerometer GPS	senspeed threshold-mod
Boulders, road geometry & dimensions	boulders	acceleration peaks orientation peaks	z-axis accelerometer x-axis gyroscope y-axis gyroscope	threshold svm c4.5
	longitudinal slope	sustained orientation change	x-axis gyroscope	miroad
		distance	GPS	
	turns	momentary orientation change	z-axis gyroscope x-axis accelerometer y-axis accelerometer	svm-multi threshold-mod
Brushwood	road softness	speed deceleration	y-axis accelerometer GPS	senspeed threshold-mod
	rutting	orientation peaks acceleration peaks	z-axis gyroscope x-axis accelerometer y-axis accelerometer	svm-multi c4.5 threshold-mod miroad
	lane changes	momentary orientation change	z-axis gyroscope x-axis accelerometer y-axis accelerometer	svm-multi c4.5 threshold-mod miroad
Bridges	surface roughness	steady vibration levels	z-axis accelerometer x-axis gyroscope y-axis gyroscope	threshold svm c4.5 lpc rqrg sobi
	bridge structure	variating vibration levels	x-axis accelerometer y-axis accelerometer z-axis accelerometer	lpc stridex
Road surface	potholes, bumps, dips	acceleration peaks orientation peaks	z-axis accelerometer x-axis gyroscope y-axis gyroscope	threshold svm c4.5
	rutting road edge verges	orientation peaks acceleration peaks	z-axis gyroscope x-axis accelerometer y-axis accelerometer	svm-multi c4.5 threshold-mod miroad

5.1.1 Road anomaly detection

The threshold-based anomaly detection systems [11, 23, 37, 20] are based on the acceleration force measurement data from the accelerometer and on the location and speed data from the GPS receiver. Acceleration measurements from a well-oriented

accelerometer sensor's z and x axes are used for the road anomaly detection. The accelerometer z-axis records the vertical and x-axis records the lateral changes in the accelerations caused from the road profile when in a moving vehicle. A series of signal processing filter algorithms (low-pass, high-pass) are used to mitigate the different sources of noise in the acceleration measurements and to filter out the normal events and result in the detect road anomaly events. Other noise mitigation approaches such as virtual reorientation [23] or active vibration recovery [37] may also be applied. Different thresholds for the acceleration force values (z,x axes), the time interval of the acceleration duration and the speed are used in the filters. A simple machine learning approach of combined brute-force search is used to find the best performing set of thresholds [11, 23, 37] for the training data. The threshold-based anomaly detection methods can be implemented as a mobile application for smartphones on Android platform as indicated by [37, 20]. The inertial sensor of a smartphone are used by default but also external device sensors can be used to obtain the acceleration and the location data. The different algorithms used in the threshold-based systems are capable of detecting whether there is a road anomaly with certain criteria (thresholds) reflected in the accelerometer data or not. But the systems, as they are described, are not capable of detecting the different types for the road anomalies (e.g. a pothole from a speed-bump) they have detected. Along with the detecting capability by collecting the road anomaly detections with the location information from multiple devices (crowdsensing) to a backend system enables the aggregation and further analysis of the anomalous events.

The scope of the detectable road anomaly types by the presented threshold-based anomaly detection method depends on the variety of the training set data which is then used to find the best scoring set of thresholds. By changing the algorithms in the different filters as suggested in [23, 37, 20], or by designing new algorithms as the filters to support for example the accelerometer y-axis data and gyroscope data, the scope of the different detectable road anomaly types can be widened. It would be interesting to experiment with more sophisticated machine learning methods to find optimal values as thresholds. Still, the detected road anomalies are a set of different types of road anomalies and further processing on the result set would be required if the different road anomaly types were to be identified. With the threshold-based anomaly detection method several different detectors could be trained, each to detect a different type of road anomaly. This could be achieved by allowing only one type of road anomalies in the training data set and by adjusting the preprocessing filter algorithms.

The threshold-based anomaly methods presented in this thesis are suitable for detecting potholes, bumps, dips, boulders, collapsed road and surface roughness as road anomalies (Tab. 5.1 *threshold*). The reasoning behind is that all of the mentioned

road anomalies are assumed to be detectable based on the accelerometer data. To detect the mentioned road anomalies the ground truth data of each of them would be required and training an independent detector for each of the anomalies is suggested.

5.1.2 Road anomaly classification

Support Vector Machine (SVM) is a supervised machine leaning method used for classification into two or more classes. When dealing with data that is expected to have considerably few data samples not belonging to the one same main class a semi-supervised learning method of the (one-class) SVM can be used [8]. When unlabelled data set is used the (one-class) SVM is considered to be unsupervised learning. For the road anomaly detection different approaches have been taken with the SVM classification [8, 25, 5, 6]. One-class SVM is used for anomaly detection where the classifier is trained with a training data set containing samples mostly of the same main class. For training a one-class SVM classifier with a Gaussian radial kernel function (RBF) the hyperparameters for the expected proportion of outliers (ν) and the smoothness of the decision boundary (γ) need to be defined. The trained model can classify new data samples either belonging to the trained class or not (anomalies). The one-class SVM was utilized in [8] with RBF and with hyperparameters $\nu = 0.01$ and $\gamma = 0.0002$. In a two-class SVM a labelled training data set containing samples from two classes is used. Similarly in multi-class SVM a labelled training data set containing samples from all of the classes is used. For training a two-class or a multi-class SVM classifier with a Gaussian radial kernel function (RBF) the hyperparameters for the smoothness of the decision boundary (γ) and the cost of misclassification soft margin need to be defined. The two-class SVM was utilized in [5, 6] with RBF and with hyperparameter $C = 10$. The exact value for the γ used in [5, 6] is not known. The two-class SVM was also utilized in [25] for the anomaly detection with RBF and hyperparameters $\gamma = 0.002$ and $C = 320$. The multi-class SVM was utilized in [25] for the anomaly classification with RBF and hyperparameters $\gamma = 0.0002$ and $C = 100$. The SVM classification results can be used for further classification as was done in [25] with two-class SVM to detect anomalies and consecutively the detected anomalies were further classified with multi-class SVM to different anomaly categories. Also in [5] the anomalies detected with a two-class SVM were further classified with a different machine learning method (Random Forest).

For road anomaly detection the data samples from the smartphone accelerometer and gyroscope sensors are used to train SVM classifier and to classify new data samples. The accelerometer data from the vertical (z) axis was used in [8, 5, 6]. A combination of accelerometer and gyroscope data was used in [25]. Even though the samples of

raw measurement data from the sensors can be used for training and classification with SVM better results are achieved with feature extraction and feature selection methods to mitigate the noise in the measurements and to obtain the best features used for training and classification. For feature extraction *window functions* with *wavelet transformations* are commonly used methods [8, 25]. The wavelet package decomposition (WPD) with *Daubechies wavelets* and 7 levels of decomposition was used to obtain the coefficients of variance as the features from the sample windows [8]. Based on analysis on the decomposed data a smaller set (30 coefficients of variance) of features were chosen as the most anomaly reflecting features to be used in the feature selection. Also empirical mode decomposition with *envelope demodulation* (Eq. 4.12) can be used to mitigate the different sources of noise in the road profile signal in the acceleration measurements [25]. The demodulated signal can be used to compute time domain features, transformed into frequency domain features (Fast Fourier Transform) and decomposed further with wavelet decomposition (Stationary Wavelet Transform). For the feature selection analysis based on experimenting with the different features to find the best performing features for the feature vector can be used [5, 25]. The sets of the time domain features, the frequency domain features and the wavelet demodulated features were selected and experimented as individual sets and as different combinations of sets to find the best performing feature vector [25]. Machine learning methods can also be used to find the best performing features [8]. Forward selection (FS), backward selection (BS), genetic algorithm (GA) and principal component analysis (PCA) were studied in [8] where PCA was found to perform the best with many features.

All the SVM classification approaches introduced in this thesis are suitable for detecting potholes, bumps, dips, boulders, collapsed road and surface roughness as road anomalies (Tab. 5.1 *svm*). The same reasoning applies here as expressed with the applicability of the threshold-based anomaly detection methods as features extracted from the accelerometer data are used to detect the road anomalies. In addition the multi-class SVM approach is suitable for detecting rutting, turns and lane-changes as road anomalies (Tab. 5.1 *svm-multi*). The reasoning here is that with the proposed multi-class SVM the gyroscope measurements could be utilized to better detect the orientation changes of the vehicle when experiencing the mentioned road anomalies. From the presented three approaches the multi-class SVM method which ulilizes both the accelerometer and gyroscope measurements to detect and classify different road anomalies (not only potholes) shows to be the most promising for road anomaly detection and classification.

5.1.3 Road roughness detection

For detecting the road surface roughness the methods such as *C4.5 Decision Tree* classifier [4], estimation with *Linear Predictive Coding* [3] and a regression model [2] have been used. The measurement data used with the *Linear Predictive Coding* detection method and the regression model based detection method is taken from the accelerometer sensor of a smartphone [3, 2]. The *C4.5 Decision Tree* classifier uses data from the accelerometer and gyroscope sensors of a smartphone [4]. The collected data is preprocessed to mitigate the noise in the measurements before the features can be extracted and selected for detection. In [4] a threshold-based low-pass filter is used to filter high-frequency measurements. The triaxial data from both sensors are transformed into time domain magnitude vectors using sliding window of size 64 values. The magnitude vectors are further converted into frequency domain vector with Fourier Fast Transform appended with the maximum magnitude values from both sensor vectors respectively. In [3] the road surface drawn with an imaginary point closely following the road surface with constant horizontal velocity is mathematically modelled as a first order low-pass filtered white Gaussian noise. In the model two parameters completely characterize the road surface profile obtained from the triaxial accelerometer measurements. The parameters are obtained by analyzing the PSD. The obtained PSD from the triaxial accelerometer measurements contain noise from many sources that hide the road profile. *Linear Predictive Coding* (LPC) is used to mitigate the noise from the measurements of all the axes and the residual prediction error for all the axes are obtained. In [2] the noise in the vertical z-axis accelerometer data is mitigated with *envelope demodulation* similarly as in [25] and to better characterize the signal from the road roughness discrete wavelet transform (DWT) is used to decompose the accelerometer signal into different frequencies. For feature selection correlation-based feature selection (CLS) was used to obtain the 24 most effective features that are used as training data for the *C4.5 Decision Tree* classifier [4]. Based on the selected features the *C4.5 Decision Tree* classifier is used to classify new data samples into two classes: *Smooth* or *Potholed*. In [3] the selected features are the residual prediction errors of the triaxial axes which are used to obtain the power prediction error estimates for each of the axes. The average of the power prediction error estimates is used as the roughness index for a road segment. In [2] the obtained coefficients form the DWT were compared against RQRG survey ratings to find the sum of local maxima points (SLM) as the explanatory variable. The SLM is used in the regression model to predict the RQRG rating as the road roughness index for the road.

As described the method used in *RoadSense* system [4] is able to classify the road samples either to anomalous and non-anomalous road. By obtaining enough ground

truth data on the different road surface roughness levels this approach could be used to build different binary classifiers with each capable of detecting a specific road roughness level. Apart from detecting the road surface roughness levels with ground truth data about different road anomaly types like potholes dips, bumps or rutting, the method used in the *RoadSense* system could also be used to train a road anomaly type specific classifiers (Tab. 5.1 *c4.5*). The method described in [3] could be used to indicate the road roughness based on accelerometer measurements. With the method also the obtained index could be used as an indicator of the structural condition of a bridge (Tab. 5.1 *lpc*). The method in [2] requires the ratings from some rating system in order to do the prediction of road roughness based on the collected accelerometer data from a road profile. Also some further analysis should be conducted to calibrate the regression model parameters for on the local environment. If such ratings would be available this method could be used for detecting the road surface roughness (Tab. 5.1 *rqrg*).

5.1.4 Driving maneuver detection

Different driving maneuvers such as right/left turn, u-turn, hard left/right turn, hard u-turn, swerve right/left are reflected in the smartphone accelerometer measurements [26]. Such driving maneuvers could be detected with similar to threshold-based anomaly detection or SVM classification methods reviewed in this thesis by customizing (tuning thresholds, training data) the methods. The Driving maneuvers can also be detected from the accelerometer, gyroscope and magnetometer measurements with Dynamic Time Warping (DTW) [17]. DTW is used to detect the different driving maneuvers from the lateral events that are reflected in the fusion of sensor data of the aforementioned sensors. The sensors data used in the fusion are the measurements from the accelerometer (y-axis), gyroscope (x-axis) and the Euler's angles (x-axis) with the help of the magnetometer measurements. Low-pass filter is used to mitigate the noise in the measurements. The simple moving average (SMA) and a suitable threshold is used to detect the event-start's and event-end's from the gyroscope data. The DWT is used to find the perfect alignment between prerecorded template event vectors and the real-time event vectors from the sensors to detect the driving maneuvers.

As mentioned above with a customized threshold-based anomaly detection or SVM classification method rutting, turns and lane changes and the speed deceleration could be detected (Tab. 5.1 *threshold-mod*) in relations with the road softness and the road roughness anomalies. Similarly the aforementioned road anomalies could be detected with the method in [17] (Tab. 5.1 *miroad*). Also with the method in [17] the sustained orientation change from the longitudinal slope for some convenient distance could be prerecorded as a template and used for detection. For the longitudinal slope

the sensors and axes to be used in the sensor data fusion would need to be found through analysis.

5.1.5 Speed detection

The speed of the vehicle can be accurately estimated by correcting the integral of the accelerometer measurements over time with the acceleration error estimates [15]. The vehicle speed at a time point is calculated from the integral of the reoriented smartphone accelerometer y-axis (axis along the vehicles's moving direction) values over time. The accelerometer measurements contains noise the simple integral results in error in the acceleration. The error in the acceleration is estimated and used to correct the speed estimation obtained from the integral. The acceleration error is obtained from the derived speeds at detected reference points during the drive. The reference points are the driving maneuvers (turns, stops) and uneven road surface events detected from the reoriented smartphone accelerometer and gyroscope measurements. Turns are detected from the gyroscope z-axis with thresholds and the speed at turn is estimated from centripetal acceleration (accelerometer) and angular velocity (gyroscope). Stops are detected from the accelerometer z-axis values with standard deviation and the speed at stops is estimated as 0. Uneven road surface is detected from the accelerometer z-axis and the speed is estimated based on observing the distance between 2 similar acceleration z-peaks with auto-correlation. By assuming the acceleration error change is small the current acceleration error is obtained from the most recent reference points with *exponential moving average*.

The accurate speed estimation method described in [15] could be used to estimate the vehicle speed to detect the speed deceleration (Tab. 5.1 *senspeed*) in relations with the road softness and the road roughness anomalies.

5.1.6 Bridge condition detection

The accelerometer measurements from a smartphone can be used to detect structural deficiencies in a bridge. The sensor data from a network of smartphone embedded sensors moving along the bridge is considered as dynamic sensor network (DSN) data which can modelled as truncated physical state-space model (TPM) [19]. The discrete-time state variables and observation variables from the TPM model are used as input to the STRIDEX algorithm. Another method for structural identification of a bridge assumes that the accelerometer measurements from a smartphone embedded sensor is a set of mixed observations consisting of vibrations from the road roughness and from the bridge structures [12]. A blind source separation algorithm Second Order Blind Identification (SOBI) is used for separating the two sources of vibrations from

the mixed observations. With the SOBI algorithm it is assumed that the vibration from the sources of the road roughness and the bridge dynamics in the mixed observations are not convoluted. To evaluate the method a virtually generated mixed observation data containing the two virtually generated sources was used. With SOBI the separated source of the vibrations for the bridge dynamics were used as input to the STRIDEX algorithm. The STRIDEX algorithm uses expectation maximization to infer the natural frequencies and the mode shapes of the bridge.

The output from the STRIDEX algorithm based the input of different smartphone accelerometer measurements of the same bridge over time could be used to monitor the condition of some of the bridges in the Finnish lower road network (Tab. 5.1 *stridex*). The applicability of the method for the bridges in the Finnish lower road network requires further analysis. It is further assumed that the road roughness profile data separated by the SOBI algorithm could be used to detect the road surface roughness (Tab. 5.1 *sobi*). Also the usability of the road roughness profile data from the SOBI algorithm requires further analysis.

5.2 Generating training data with GANs

Generative Adversarial Nets (GANs) is a framework to estimate generative models with an adversarial process introduced by Goodfellow, Pouget-Abadie, Mirza, Xu, Warde-Farley, Ozair, Courville and Bengio [13]. A generative model (G) captures the data distribution to generate samples and a discriminative model (D) estimates the probability that the sample was generated by G or came from the training data. During the process the G model learns to improve the generated samples by taking feedback from the D model. Also during the process the D model learns to improve the discrimination between the generated samples and the known training data. The process goes on until the G model has learned to generate samples that are so improved that the model D can not discriminate the generated samples from the known training data.

The absence of ground truth data about different road anomalies to be used in the training of the detectors have been mentioned by many [35, 8, 25, 23, 11, 6]. To the problem was mitigated in P^2 [11] by extending the training data set with additional *loosely labelled* data. And in [6] the *PotholeLab* was introduced to generate virtual roads by concatenating previously collected anomalous and non-anomalous road data. *PotholeLab* is publicly available and one of the reasons behind it was to offer data with same quality for evaluation of the different road condition detection approaches. The problem with these two approaches are that both take the data of previously collected road anomalies and make multiple copies of same road anomaly instances.

To obtain more novel ground truth data of the different road anomalies the use of

the GANs framework of competing generative and discriminative models would be an interesting approach to be analyzed. The discriminative model would still need some amount of diverse ground truth data about to be able to learn to discriminate between the generated samples and the training data. The raw sensor data for example from the accelerometer contains the characteristics of the different sources of noise along with the characteristics of the road anomaly. The noise characteristics depend on the setup of devices and vehicles used for collecting the initial ground truth data. Mitigating the noise from the data might seem useful so that the discriminative model would not be guiding the generative model with the features from the noise. The novel road anomaly samples generated with a GANs model would need to be analysed whether they could help in training the kind of road anomaly detectors discussed in this thesis.

5.3 Predicting road condition with WaveNet

WaveNet is a generative model for generating raw audio waveforms presented by van den Oord, Dielman, Zen, Simonyan, Vinyals, Graves, Kalchbrenner, Senior and Kavukcuoglu [30]. The model is a convolutional neural network trained with the input sequences of raw audio waveform samples. In raw audio there are typically 16 000 samples per second. The *WaveNet* model predicts new raw audio samples with each conditioned on all previous samples. The model can be conditioned with other input to guide the generation of raw audio sample with the required characteristics. A *WaveNet* model was trained with multi-speaker English corpus and was conditioned on one of the speakers the model generated human-like non-language words with perfect sounding intonations of the conditioned speaker. This indicates that *WaveNet* is able capture the characteristics of all the different speakers of the corpus. It was also observed that when speakers were added the performance was better than with less or only one speaker. This indicates that *WaveNet's* internal representation is shared with the other speakers. Also other characteristics such as acoustics and recording quality from the input raw audio waveform were present in the generated samples. Experimenting with music a model was trained with raw audio waveform of classical piano with no conditioning and the model was found to generate novel and highly realistic samples of music. Another *WaveNet* model trained with single-speaker dataset and conditioned with the *linguistic features* inferred from input texts. The generated samples of text-to-speech outperformed the best TTS systems in subjective naturalness of the generated speech. Generative *WaveNet* can also be adapted to discriminative tasks like speech recognition.

The capabilities of the *WaveNet* generative model with the raw audio waveform data makes one wonder would the model work with other types of waveform data. The

vibrations from the road surface obtained for example by an accelerometer from the three axes are a type of waveform. It would be interesting from the road condition estimation point of view to analyze that could the *WaveNet* model be used to predict road conditions. Assuming with a large enough time series of accelerometer data from a certain road or a road network with good spatial coverage the raw accelerometer waveform data could be used to train a *WaveNet*-like model. As seen in this thesis the accelerometer data contains the characteristics of the road profile (roughness, potholes, dips, weather, time, etc.) along with the characteristics of the vehicle (probing wheel, suspension system, dampening, speed, etc.) and the smartphone device (phone type, orientation, sensor components, etc.) or even the driver (driving maneuvers, driving behaviour). One can imagine that without conditioning the model would predict the next accelerometer samples, based on all the previous samples, to form a novel raw accelerometer waveform for a non-existing road. Quickly thinking it does not make sense to generate data to non-existing road but the generated novel data would still represent some kind of generalised view of the input data in the model. Could that representation reflect the current conditions of the road (or road network). Or perhaps the result would be something as fantastic as with music [30]. Better and more useful results would be obtained by using proper conditioning, but the question of course is what are the proper conditioning features: driver, vehicle type, suspension system, dampener. Even with those, valuable information could be obtained of such characteristics. For generating the road conditions the raw input data would probably need to be tagged with additional information like location information and timestamp of each sample, and the addition or the fusion of other sensor data like from the gyroscope. Also the discriminative capability of *WaveNet* could be proved useful in detecting the different types of road anomalies from the raw accelerometer waveform.

6. Conclusions

This thesis the covers rationale for the importance of the timely road condition data of the lower road network for the Finnish forest industry. The road transportation is the most important long-distance transportation method of the domestic wood and therefore the majority of the long-distance transportation costs are road transportation related. The poor condition of the lower road network is seen as one of the biggest factors increasing the wood transportation costs as the wood transportation by road is carried mainly on the lower road network. The total size of the Finnish road network is approximately 454 000 km, most of it is covered by the lower road network with 77 % of the total road network being private roads. Timely information about road conditions of the lower road network is required for the wood transportation planning and the road maintenance to reduce the road transportation related costs.

Based on the relevant prior research programs and pilots the method of crowdsourcing to collect the timely road conditions data from the lower road network, including forest roads, has been considered. Modern day smartphones with the sensing, computing and networking capabilities are suitable platform to collect, analyze and share the road conditions data. With a mobile application the road conditions data can be collected by any smartphone owner without the need of specialist personnel. This is a very straight-forward idea, however incentivising the common people to collect the data might be challenging if there is no clear benefit for them to collect the data. Therefore the crowdsourcing could still be limited to those who are required to collect the data or can do the collecting at on the side of some other task being performed on the road. Nevertheless utilizing smartphones and *piggyback*-crowdsourcing to collect road conditions data is relatively inexpensive in comparison to specialist hardware and labor.

The road condition factors that are used in the visual assessment of the forest road conditions are presented in this thesis. For each road condition factor the related road anomalies are presented and the how those road anomalies are assumed to be reflected on the smartphone embedded inertial sensor's measurements have been analyzed. With considering some of the practicalities in sensing the road anomaly reflections with a smartphone the different existing computational methods for detecting

the road anomalies are reviewed. From the reviewed methods the threshold-based and SVM classification are mostly suited for detecting the abrupt road anomalies on the road surface such as potholes, dips, bumps and etc. Road surface roughness, driving maneuvers, bridge structure, vehicle speed and turns would require more customized approach. The preprocessing of the inertial sensor measurements is an important prior step to mitigate the different sources of noise for all of the computational methods reviewed. Summary of the road condition factors and the most suitable method for detecting the road anomalies in each is suggested in this thesis.

From the reviewed detection methods the author of this thesis is interested to analyse the following methods further in practice on Finnish lower road network. The *RoADS* system [25] approach with multi-class SVM to detect different types of road anomalies. The *RoadSense* system [4] approach with *C4.5 Decision Tree* for the road surface roughness detection. The *MIROAD* system [17] approach with the DTW for detecting driving maneuvers. The *SenSpeed* system [15] approach for the accurate speed estimation. And finally the SOBI approach with STRIDEX algorithm [12] for obtaining information on structural bridge condition and road surface roughness. Additionally, further interest lies in analysing he topics on the use of GANs for generating more ground truth data for training the detection methods and the use of WaveNet model for predicting the future condition of roads.

Bibliography

[1] Akansu, A. N., Serdijn, W. A., and Selesnick, I. W. Emerging applications of wavelets: A review. *Physical Communication 3*, 1 (2010), 1 – 18.

[2] Aleadelat, W., Wright, C. H. G., and Ksaibati, K. Estimation of gravel roads ride quality through an android-based smartphone. *Transportation Research Record 2672*, 40 (2018), 14–21.

[3] Alessandroni, G., Klopfenstein, L. C., Delpriori, S., Dromedari, M., Luchetti, G., Paolini, B. D., Seraghiti, A., Lattanzi, E., Freschi, V., Carini, A., and Bogliolo, A. Smartroadsense: Collaborative road surface condition monitoring. *UBICOMM 2014, The Eighth International Conference on Mobile Ubiquitous Computing, Systems, Services and Technologies*, 6 (August 2014), 210–215.

[4] Allouch, A., Koubâa, A., Abbes, T., and Ammar, A. Roadsense: Smartphone application to estimate road conditions using accelerometer and gyroscope. *IEEE Sensors Journal 17*, 13 (July 2017), 4231–4238.

[5] Aragón, M. E., Carlos, M. R., González-Gurrola, L. C., and Escalante, H. J. A machine learning pipeline to automatically identify and classify roadway surface disruptions. In *Proceedings of the Sixteenth Mexican International Conference on Computer Science* (New York, NY, USA, 2016), ENC '16, ACM, pp. 3:1–3:4.

[6] Carlos, M. R., Aragón, M. E., González, L. C., Escalante, H. J., and Martínez, F. Evaluation of detection approaches for road anomalies based on accelerometer readings - addressing who's who. *IEEE Transactions on Intelligent Transportation Systems 19*, 10 (Oct 2018), 3334–3343.

[7] Chang, C.-C., and Lin, C.-J. Libsvm: A library for support vector machines. *ACM Trans. Intell. Syst. Technol. 2*, 3 (May 2011), 27:1–27:27.

[8] CONG, F., HAUTAKANGAS, H., NIEMINEN, J., MAZHELIS, O., PERTTUNEN, M., RIEKKI, J., AND RISTANIEMI, T. Applying wavelet packet decomposition and one-class support vector machine on vehicle acceleration traces for road anomaly detection. In *Advances in Neural Networks – ISNN 2013* (Berlin, Heidelberg, 2013), C. Guo, Z.-G. Hou, and Z. Zeng, Eds., Springer Berlin Heidelberg, pp. 291–299.

[9] DATABIO. Data-driven Bioeconomy. https://www.databio.eu/en/, last accessed on 01.06.2019.

[10] DIMECC. Data to Intelligence. http://www.datatointelligence.fi/, last accessed on 01.06.2019.

[11] ERIKSSON, J., GIROD, L., HULL, B., NEWTON, R., MADDEN, S., AND BALAKRISHNAN, H. The pothole patrol: Using a mobile sensor network for road surface monitoring. In *Proceedings of the 6th International Conference on Mobile Systems, Applications, and Services* (New York, NY, USA, 2008), MobiSys '08, ACM, pp. 29–39.

[12] ESHKEVARI, S. S., AND PAKZAD, S. N. Bridge structural identification using moving vehicle acceleration measurements. In *Dynamics of Civil Structures, Conference Proceedings of the Society for Experimental Mechanics Series* (Cham, June 2018), vol. 2, Springer, pp. 251–261.

[13] GOODFELLOW, I. J., POUGET-ABADIE, J., MIRZA, M., XU, B., WARDE-FARLEY, D., OZAIR, S., COURVILLE, A. C., AND BENGIO, Y. Generative adversarial nets. In *Advances in Neural Information Processing Systems 27: Annual Conference on Neural Information Processing Systems 2014, December 8-13 2014, Montreal, Quebec, Canada* (2014), pp. 2672–2680.

[14] GOOGLE. Android Developers - Sensors. https://developer.android.com/guide/topics/sensors/index.html, last accessed on 01.06.2019.

[15] HAN, H., YU, J., ZHU, H., CHEN, Y., YANG, J., ZHU, Y., XUE, G., AND LI, M. Senspeed: Sensing driving conditions to estimate vehicle speed in urban environments. In *IEEE INFOCOM 2014 - IEEE Conference on Computer Communications* (April 2014), pp. 727–735.

[16] HOLM, P., HIETALA, J., AND HÄRMÄLÄ, V. Transport network and economy: Cross-country comparison between finland and sweden. *PTT Reports 249* (2015).

[17] Johnson, D. A., and Trivedi, M. M. Driving style recognition using a smartphone as a sensor platform. In *2011 14th International IEEE Conference on Intelligent Transportation Systems (ITSC)* (Oct 2011), pp. 1609–1615.

[18] Korpilahti, A. Metsäteiden kuntoinventoinnin ja kuntotiedon hyödyntämisen toimintamalli. *Metsätehon raportti 202* (2008).

[19] Matarazzo, T., Vazifeh, M., Pakzad, S., Santi, P., and Ratti, C. Smartphone data streams for bridge health monitoring. *Procedia Engineering 199* (2017), 966 – 971. X International Conference on Structural Dynamics, EURODYN 2017.

[20] Mednis, A., Strazdins, G., Zviedris, R., Kanonirs, G., and Selavo, L. Real time pothole detection using android smartphones with accelerometers. In *2011 International Conference on Distributed Computing in Sensor Systems and Workshops (DCOSS)* (June 2011), pp. 1–6.

[21] Metsäkeskus. Yksityistietiedon palvelualusta. https://www.metsakeskus.fi/biotalouden-tietojarjestelma, last accessed on 01.06.2019.

[22] Metsäkeskus. Metsätietieto web map service. https://www.arcgis.com/apps/webappviewer/index.html?id=ffdfc0c038da44399fb6e33c15cc44d3, last accessed on 01.06.2019.

[23] Mohan, P., Padmanabhan, V. N., and Ramjee, R. Nericell: Rich monitoring of road and traffic conditions using mobile smartphones. In *Proceedings of the 6th ACM Conference on Embedded Network Sensor Systems* (New York, NY, USA, 2008), SenSys '08, ACM, pp. 323–336.

[24] RoadsML. Crowdsourcing mobile application. https://roadsml.com/, last accessed on 01.06.2019.

[25] Seraj, F., van der Zwaag, B. J., Dilo, A., Luarasi, T., and Havinga, P. Roads: A road pavement monitoring system for anomaly detection using smart phones. In *Big Data Analytics in the Social and Ubiquitous Context* (Cham, 2016), M. Atzmueller, A. Chin, F. Janssen, I. Schweizer, and C. Trattner, Eds., Springer International Publishing, pp. 128–146.

[26] Singh, P., Juneja, N., and Kapoor, S. Using mobile phone sensors to detect driving behavior. In *Proceedings of the 3rd ACM Symposium on Computing for Development* (New York, NY, USA, 2013), ACM DEV '13, ACM, pp. 53:1–53:2.

[27] STOICA, P., AND MOSES, R. *Spectral Analysis Of Signals*. Pearson-Prentice Hall, 2005.

[28] STRANDSTRÖM, M. Timber harvesting and long-distance transportation of roundwood 2017. *Metsätehon tuloskalvosarja 8b/2018* (2018).

[29] VÄÄTÄINEN, K., ANTTILA, P., LAITILA, J., NUUTINEN, Y., AND ASIKAINEN, A. Aines- ja energiapuun kaukokuljetuksen tulevaisuuden haasteet ja teknologiat. *Metlan työraportteja / Working Papers of the Finnish Forest Research Institute 291* (2014).

[30] VAN DEN OORD, A., DIELEMAN, S., ZEN, H., SIMONYAN, K., VINYALS, O., GRAVES, A., KALCHBRENNER, N., SENIOR, A. W., AND KAVUKCUOGLU, K. Wavenet: A generative model for raw audio. *CoRR abs/1609.03499* (2016).

[31] VAYLA. Digiroad Database. https://vayla.fi/web/en/open-data/digiroad#.XPJBd9Mza-s, last accessed on 01.06.2019.

[32] VAYLA. The Finnish road network. https://vayla.fi/web/en/road-network#.XGheAZMzZZg, last accessed on 01.06.2019.

[33] VENÄLÄINEN, P., ALANNE, H., OVASKAINEN, H., POIKELA, A., AND STRANDSTRÖM, M. Kausivaihtelun kustannukset ja vähentämiskeinot puun toimitusketjussa. *Metsätehon tuloskalvosarja 8/2017* (2017).

[34] VENÄLÄINEN, P., RÄSÄNEN, T., AND HÄMÄLÄINEN, J. Tiestödatan nykytila, visio ja toimenpideohjelma: Forest big data -hankkeen osaraportti. *Metsätehon raportti 239* (2016).

[35] VENÄLÄINEN, P., RAUTEVAARA, A., PIHLAJISTO, I., MELANDER, M., HIENONEN, P., HÄMÄLÄINEN, J., AND STRANDSTRÖM, M. Tilannekuva ja automatisoitu tiedontuotanto metsäsektorin kuljetuksista. *Metsätehon raportti 244* (2017).

[36] WAIKATO. Waikato Environment of Knowledge Analysis. https://www.cs.waikato.ac.nz/~ml/weka/index.html, last accessed on 01.06.2019.

[37] XUE, G., ZHU, H., HU, Z., YU, J., ZHU, Y., AND LUO, Y. Pothole in the dark: Perceiving pothole profiles with participatory urban vehicles. *IEEE Transactions on Mobile Computing 16*, 5 (May 2017), 1408–1419.